HEDL-TME 72-93

Gas Tag Burnup Analysis for Fuel Failure Location and Detection in the FTR

MASTER

Hanford Engineering Development Laboratory

Contract:
AT(45-1)-2170

DISCLAIMER

NOTICE

Hanford Engineering Development Laboratory

Richland, Washington

operated by

WestinghouseHanford Westinghouse Hanford Company
A subsidiary of Westinghouse Electric Corporation

for the

United States Atomic Energy Commission

Under Contract No. AT(45-1)-2170

HEDL-TME 72-93

Gas Tag Burnup Analysis for Fuel Failure Location and Detection in the FTR

Hanford Engineering Development Laboratory

E. T. Boulette

R. E. Schenter

F. Schmittroth

July, 1972

Contract:
AT(45-1)-2170

ABSTRACT

Calculations were made to determine time-dependent ratio changes of noble gas isotopes being considered for use as tags for fuel failure detection and location in the Fast Test Reactor (FTR). The ratio changes occur due to neutron capture by the individual tag gas isotopes. Results are presented for the FTR as a function of exposure time. Analyses extending over the average lifetime of a fuel assembly are given for seven isotopes of interest: ^{78}Kr, ^{80}Kr, ^{82}Kr, ^{124}Xe, ^{126}Xe, ^{128}Xe and ^{129}Xe. Uncertainties in the calculations, as propagated from uncertainties in the capture cross sections and neutron flux distributions, are also included.

TABLE OF CONTENTS

ILLUSTRATIONS

ILLUSTRATIONS (CONT)

TABLES

I. INTRODUCTION

The ability to locate rapidly a failed fuel assembly in a nuclear reactor is of significant importance to the efficient operation of the facility. A method under consideration for use in the Fast Test Reactor (FTR) consists in "tagging" each fuel assembly with a unique isotopic mixture of a noble gas, such as xenon or krypton. In the event one or more of the pins in an assembly fails, the tag gas is emitted; and, by means of mass spectrometer measurements on the gas, the failed assembly may be located. Locating failed assemblies with the gas tag method will be most efficient if each assembly contains a unique tag throughout its lifetime. Since the tags will be exposed to a relatively large neutron flux during FTR operation, the isotopic composition of the tags will change with exposure time because of neutron capture. Therefore, the selection of gas tag compositions will be dependent upon the neutron capture rate of the individual tag isotopes.

The noble gas isotopes being considered for use as tags in the FTR are ^{78}Kr, ^{80}Kr, ^{82}Kr, ^{124}Xe, ^{126}Xe, ^{128}Xe and ^{129}Xe. This report presents burnup analyses as a function of exposure time for certain mixtures of these isotopes. Uncertainties in the burnup analyses due to uncertainties in the neutron flux and capture cross sections are also presented.

II. SUMMARY

Burnup analyses are presented for the following isotopic ratios:

1. $^{129}Xe/^{124}Xe$
2. $^{128}Xe/^{124}Xe$
3. $^{128}Xe/^{126}Xe$
4. $^{129}Xe/^{128}Xe$
5. $^{80}Kr/^{78}Kr$
6. $^{82}Kr/^{78}Kr$
7. $^{82}Kr/^{80}Kr$

Results indicate that five of these isotopic ratios will change by less than 15% over an FTR fuel assembly lifetime. The ratios involving ^{124}Xe change by more than a factor of two. Large changes in isotopic ratios are undesirable because they limit the number of potential tags. Conversely, tags identified by the $^{128}Xe/^{126}Xe$ ratio tend to be more desirable because their

ratios are expected to change by less than 3% over an assembly lifetime.

The time variation of $^{129}Xe/^{128}Xe$ ratios is shown to be essentially unaffected by the production of ^{129}Xe due to neutron capture in ^{128}Xe for ratios greater than 0.1. $^{129}Xe/^{128}Xe$ ratios smaller than 0.1, however, must include a ^{129}Xe production term which is linear in time over the fuel assembly lifetime and directly proportional to the microscopic neutron capture rate in ^{128}Xe.

III. RESULTS AND DISCUSSION

A. BACKGROUND

The present FTR design includes 73 fuel assemblies. In the event of a fuel assembly failure (detected by monitoring of the cover gas for fission product release), the FTR will be shut down and steps for locating the failed element will be initiated. Several methods for locating failed assemblies are possible. One method, a shuffling approach, consists in replacing a number of assemblies in the core with new assemblies, bringing the FTR to power, and monitoring the cover gas for fission product release. If no fission product release is detected, the failed assembly is presumed to be among those just removed. If fission product release is detected, the failed assembly is still located in the core, and another group of assemblies must be replaced. The procedure is repeated until the failed assembly is located. Obviously, this assembly shuffling approach implies a significant amount of "down time," which reduces the overall efficiency of the FTR.

An alternate method for locating failed fuel assemblies in the FTR is the "gas tag method." In this method, each fuel assembly is tagged with a unique isotopic mixture of a noble gas, such as xenon or krypton. These gas tags are to be loaded into the fission gas plenums of each fuel assembly. Locating a failed assembly is accomplished by sampling the gas evolved and

determining its isotopic mixture by mass spectrometer analyses. Experimentation[1] with this method has been done and was shown to be successful.

The gas tag method is most efficient if each fuel assembly contains a unique tag throughout its lifetime. Any tag redundancy necessitates an additional step (possibly the shuffling approach described above) for locating the failed assembly. The isotopic mixture of the tags will vary with exposure to neutron flux because the neutron capture rates of the isotopes are different. Consequently, the manner in which the tag compositions change with exposure time influences the selection of the initial tag compositions.

B. NEUTRON FLUX DISTRIBUTION

An FTR fuel assembly contains 217 eight-foot long fuel pins. The top 42 inches of each of these pins are filled initially with an inert gas and constitute the expansion chambers for containing fission product gases produced by fission in the fuel. The gas tags are to be inserted into these fission gas plenums. To evaluate the time variation of the tag compositions, calculations of the neutron flux distribution in the fission gas plenum region were made with the two-dimensional diffusion theory code 2DBS[2]. The neutron transport cross sections were taken from the 31-group HOMSET[3] cross section library. An R-Z geometrical model was assumed and the results were normalized to a core power of 400 MW. In Figure 1 is shown the map of material zones used in the analyses. The material composition of each zone is listed in Table 1. The fission gas plenum zone was treated as a homogeneous region. Monte Carlo analyses[4] were made which indicate a homogeneous representation of the plenum region is adequate; i.e., neutron streaming through the gas-filled expansion chambers of each fuel pin is insignificant.

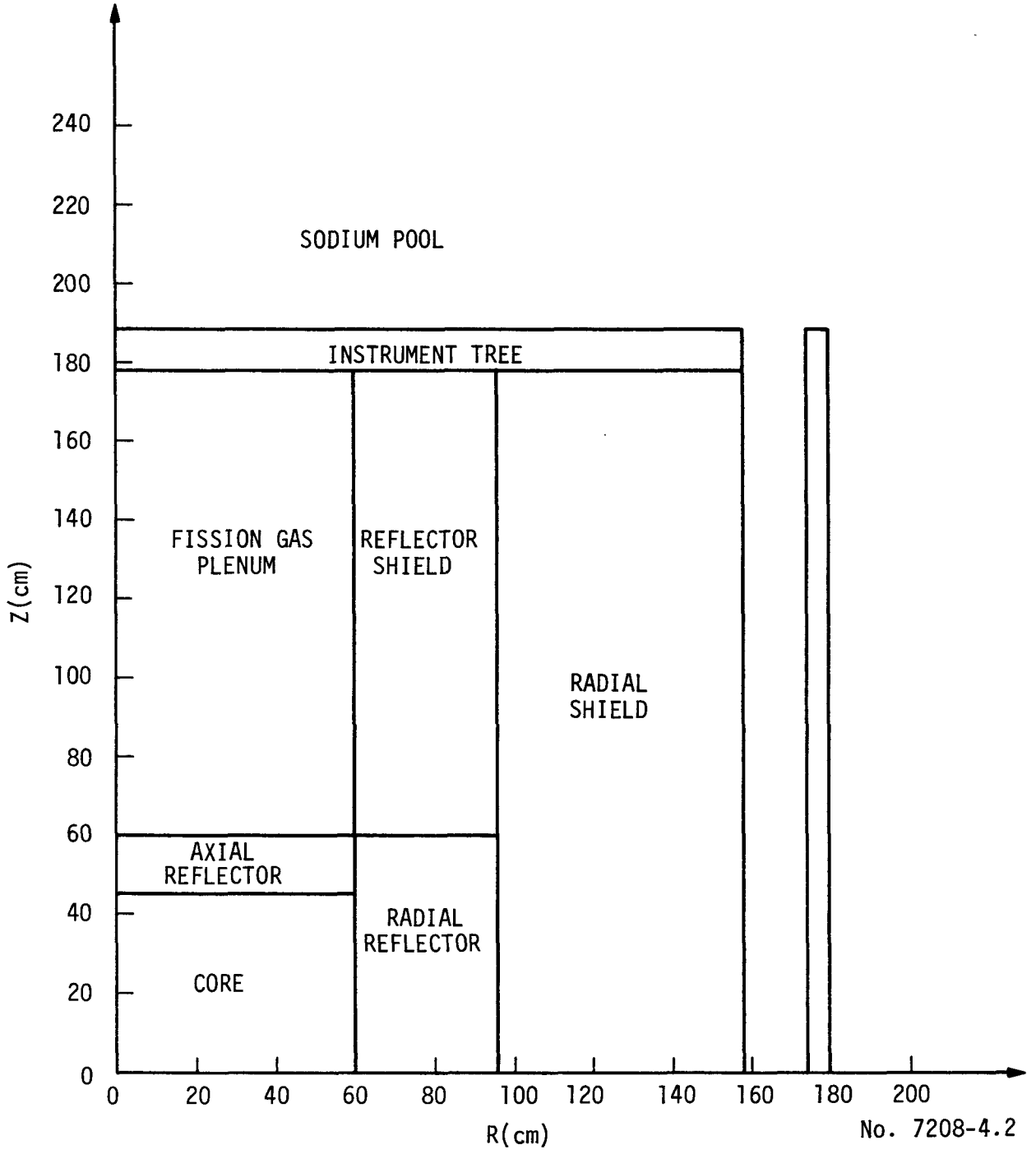

Figure 1. Map of Material Zones

TABLE 1

Material Composition by Zone (V/O)

Zone	Fuel	SS	Na	Inconel
Core	34.76	24.46	40.78	0.0
Axial Reflector	0.0	24.46	40.78	34.76
Radial Reflector	0.0	12.6	10.2	77.2
Fission Gas Plenum	0.0	24.26	40.78	0.0
Radial Shield	0.0	96.75	3.25	0.0
Instrument Tree	0.0	20.18	79.82	0.0
Reflector Shield	0.0	89.8	10.2	0.0

The neutron spectral distribution was calculated at more than 200 locations in the plenum region. In Figure 2 are plotted the neutron spectra along the centerline of the plenum region. Results are presented at three elevations; the bottom of the plenum region, the mid-plane elevation, and the top of the region. Also included in Figure 2 is the neutron spectrum averaged over the volume of the fission gas plenum region. The volume-averaged group flux per unit lethargy is defined as

$$\bar{\phi}_I/\Delta u_I = \frac{\int_V (\phi_I/\Delta u_I)\,dV}{\int_V dV} \quad ,$$

where V is the volume of the fission gas plenum region, and Δu_I is the lethargy width in group I of the HOMSET library. (The lethargy width for each group is listed in Table 2.) The volume-averaged total flux is then defined as

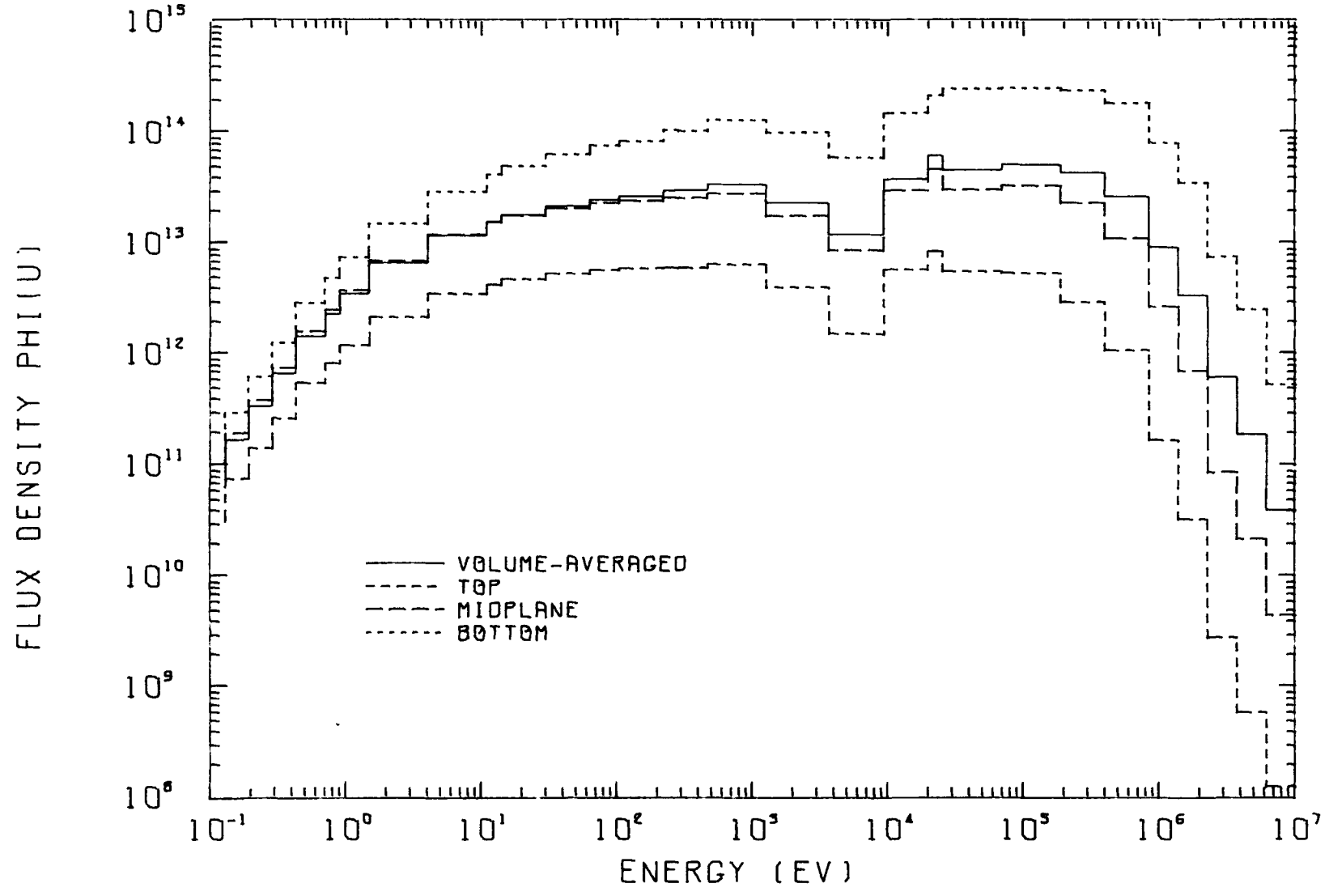

Fig. 2 FTR Fission Gas Plenum Spectra

TABLE 2

HOMSET 31-Group Structure

GP	E Upper		E Lower		Δu
1	10.0	MeV	6.065	MeV	0.500
2	6.065	MeV	3.679	MeV	0.500
3	3.679	MeV	2.231	MeV	0.500
4	2.231	MeV	1.353	MeV	0.500
5	1.353	MeV	0.8209	MeV	0.500
6	820.9	keV	387.7	keV	0.750
7	387.7	keV	183.2	keV	0.750
8	183.2	keV	67.38	keV	1.000
9	67.38	keV	24.79	keV	1.000
10	24.79	keV	19.3	keV	0.250
11	19.3	keV	9.119	keV	0.750
12	9.119	keV	3.355	keV	0.942
13	3.355	keV	1.234	keV	1.058
14	1.234	keV	0.454	keV	1.649
15	454.0	eV	275.4	eV	0.500
16	275.4	eV	214.5	eV	0.250
17	214.5	eV	101.3	eV	0.750
18	101.3	eV	61.44	eV	0.500
19	61.44	eV	29.02	eV	0.750
20	29.02	eV	13.71	eV	0.750
21	13.71	eV	10.68	eV	0.250
22	10.68	eV	3.928	eV	1.000
23	3.928	eV	1.445	eV	1.000
24	1.445	eV	0.8764	eV	0.500
25	0.8764	eV	0.6826	eV	0.250
26	0.6826	eV	0.4140	eV	0.500
27	0.4140	eV	0.2775	eV	0.400
28	0.2775	eV	0.1860	eV	0.400
29	0.1860	eV	0.1247	eV	0.400
30	0.1247	eV	0.07595	eV	0.496
31	0.07595	eV	0.0	eV	-----

$$\bar{\phi}_T = \sum_{I=1}^{31} \bar{\phi}_I \quad .$$

The uncertainty in the neutron flux calculations was estimated from analyses[3,5,6] of FTR shielding experiments. It is estimated that the calculated neutron flux, in the energy range of interest, is uncertain by about 15% at the "68% confidence limits." Further analyses of experiments will be factored into these results as they are completed.

C. CROSS SECTION CALCULATIONS

Microscopic Cross Sections

Since essentially no experimental data exist for the capture cross sections of the tag gas isotopes, cross section calculations were made combining a statistical model treatment (Hauser-Feshbach formalism[7] with fluctuation corrections) with known resonance parameter information[8-10], integral data[11,12] and thermal measurements[13,14]. Contributions from bound levels were also estimated for the situation in which resonance parameter and thermal values were not in agreement.

For the Hauser-Feshbach calculations, use was made of recent investigations[15] on the average resonance spacing, D_{obs} for each of a large number of nuclei. Resolved neutron resonance data were analyzed for about 100 nuclei and computer studies were made to relate D_{obs} with the level density parameter $\underline{a}$. The expected systematic behavior of $\underline{a}$ with mass number A can then be used to interpolate the unknown cases. The above procedure was used to find D_{obs} for all the tag gas isotopes except ^{129}xenon, which is the only one to have had more than its lowest energy resonance measured[9,10].

In addition to calculating the capture cross sections, quantitative estimates were made of the uncertainties in the cross section results. In many cases the Hauser-Feshbach calculations were extended necessarily to low energies where large fluctuations could be expected in the results[16]. These fluctuations, taken together with the uncertainties associated with resonance parameter information, integral data, thermal data and the input data for the Hauser-Feshbach calculations, were used to obtain the final error estimates. A detailed description of the energy-dependent cross section calculations and their uncertainties is given in Reference 17.

Spectrum Averaged Cross Sections

In order to calculate correctly capture reaction rates for each energy group, energy-dependent capture cross sections were integrated over an assumed flux distribution of the form†

$$\phi(E) = AE^{-\alpha} \qquad \text{(C-1)}$$

where α varies from group to group. The values of α were calculated using the flux results from the 2DBS run described in the previous section.

Table 3 gives the α values by group for three plenum positions and the volume-averaged plenum. With Equation (C-1), group-averaged capture cross sections are then given as

---

† Standard infinitely dilute multigroup cross sections correspond to using $\alpha = 1$ (Fermi Spectrum). Modifying the usual 1/E form is an important correction for the gas plenum calculations. For most of the isotopes, a large percentage of their reaction rate comes from their low energy resonances, where the flux is significantly different from the Fermi shape. For example, a 20% error in the ^{124}Xe reaction rate would result if the standard 1/E spectrum were used.

TABLE 3

Group Flux Density Parameter α_I For Positions In The FTR Gas Plenum

Group I	Top	Midplane	Bottom	Volume-Averaged
1	5.3	5.3	5.3	5.3
2	4.2	4.0	3.7	3.7
3	5.0	4.5	3.6	3.9
4	5.1	4.4	3.4	3.7
5	4.6	3.9	2.8	3.2
6	2.8	2.4	1.6	1.9
7	2.1	1.8	1.3	1.5
8	1.3	1.1	.93	.95
9	1.1	1.0	.74	.93
10	2.3	2.2	1.3	1.9
11	- .28	- .27	.01	- .25
12	.78	.71	.77	.73
13	1.6	1.5	1.3	1.5
14	1.1	1.1	.91	1.0
15	1.1	1.0	.94	.99
16	1.7	1.6	1.3	1.5
17	.70	.67	.52	.62
18	1.2	1.1	.99	1.0
19	.79	.73	.61	.70
20	.69	.65	.57	.63
21	1.6	1.5	1.2	1.4
22	.46	.39	.28	.36
23	.35	.30	.21	.28
24	.20	.14	.02	.11
25	- .03	- .18	- .40	- .24
26	- .32	- .40	- .51	- .43
27	- .64	- .74	- .87	- .78
28	- .56	- .69	- .84	- .72
29	- .86	-1.0	-1.2	-1.0
30	-1.0	-1.2	-1.4	-1.2
31	-1.0	-1.2	-1.4	-1.2

$$\sigma_{n\gamma}^{I} = \int^{I} E^{-\alpha_I} \sigma_{n\gamma}(E)\, dE \Big/ \int^{I} E^{-\alpha_I}\, dE \quad . \qquad \text{(C-2)}$$

Figures 3-9 show the group cross sections $\sigma_{n\gamma}^{I}$ for the xenon and krypton isotopes for the volume-averaged plenum spectrum.

Table 4 gives spectrum-averaged capture cross sections, $\bar{\sigma}_{n\gamma}$, for the three plenum positions and the volume-averaged plenum. $\bar{\sigma}_{n\gamma}$ is defined in terms of the total capture reaction rate as

$$\bar{\sigma}_{n\gamma} = \sum_{I=1}^{31} \sigma_{n\gamma}^{I} \bar{\phi}_I \Big/ \bar{\phi}_T \quad . \qquad \text{(C-3)}$$

Also included in Table 4 are calculated estimates of the uncertainty for the $\bar{\sigma}_{n\gamma}$ values. The $\pm$ notation specifies the usual 68% (1σ for a Normal distribution) confidence interval. The nonsymmetric interval limits for large uncertainties reflect the fact that the distribution function for $\bar{\sigma}_{n\gamma}$ is not Normal. See Reference 17 for a more detailed discussion of this point.

D. TIME VARIATION OF GAS TAG RATIOS

The isotopic ratio that identifies a tag will vary with exposure to neutron flux. To establish the initial mixture compositions and assure that the tag ratios remain unique over the fuel assembly lifetime, it is necessary to know the burnup rate of each isotope and to be able to predict the variation of the isotopic ratio of each tag as a function of exposure time.

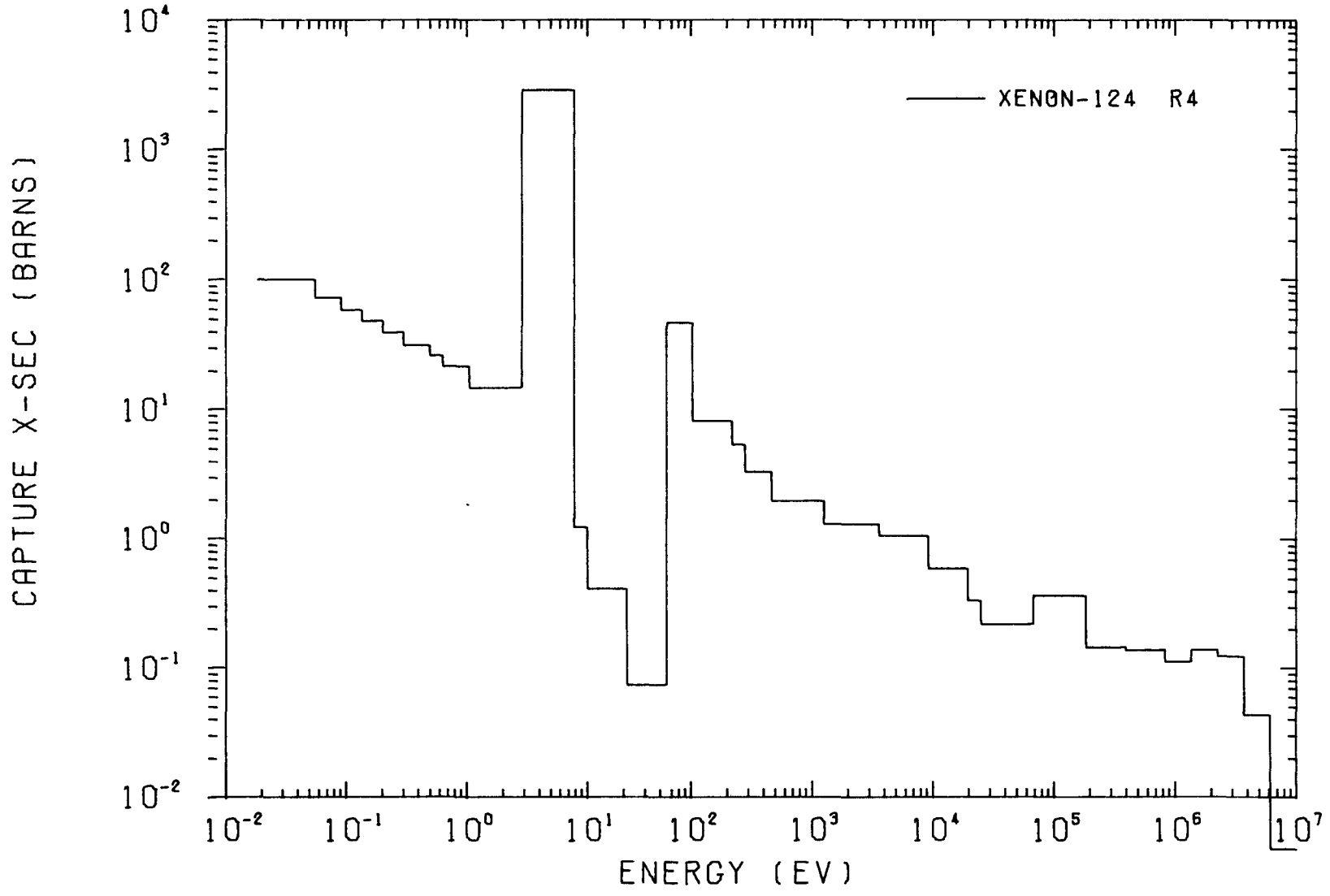

Figure 3. ^{124}Xe Spectrum Weighted Group Capture Cross Sections for the Volume-Averaged Plenum

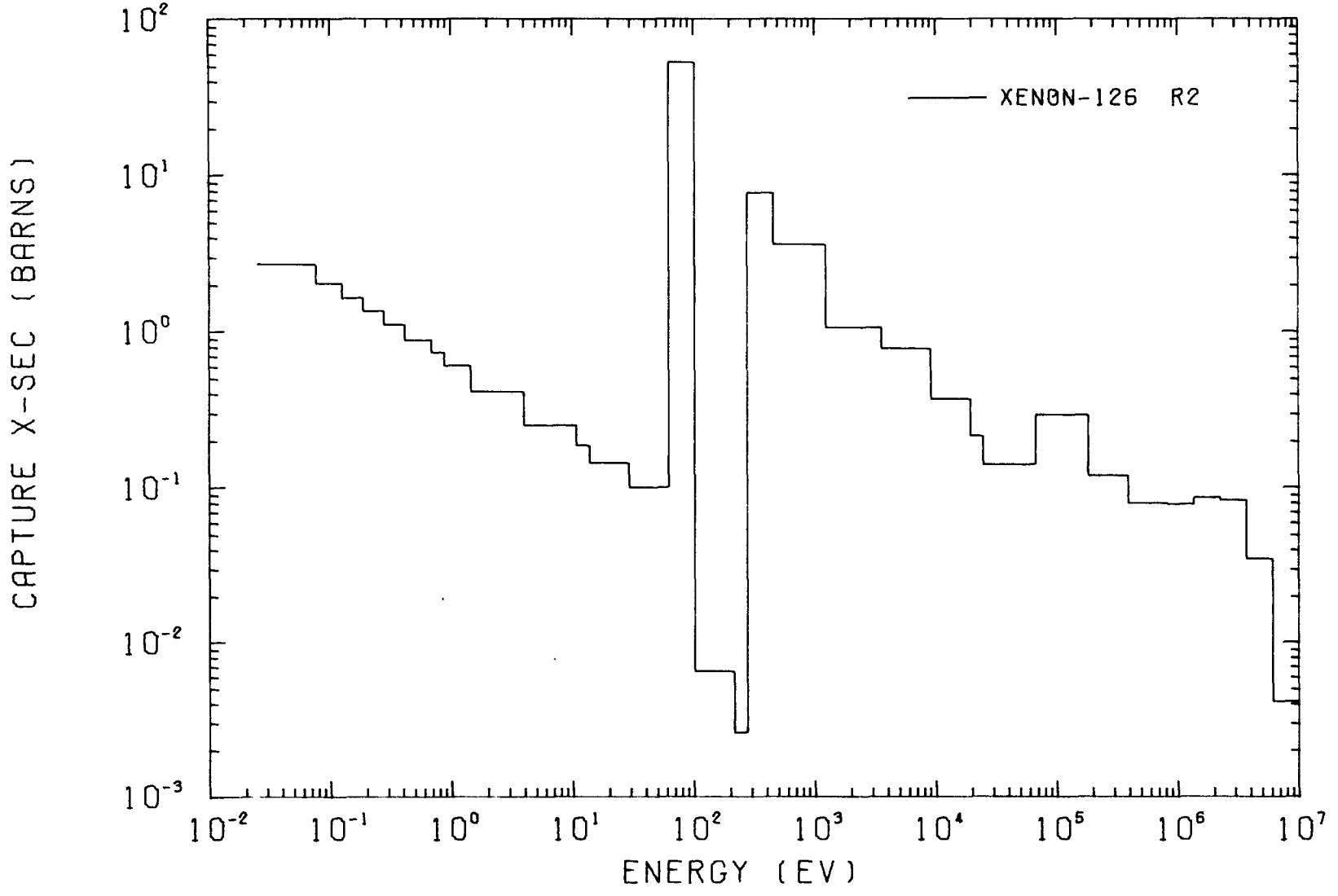

Figure 4. ^{126}Xe Spectrum Weighted Group Capture Cross Sections for Volume-Averaged Plenum

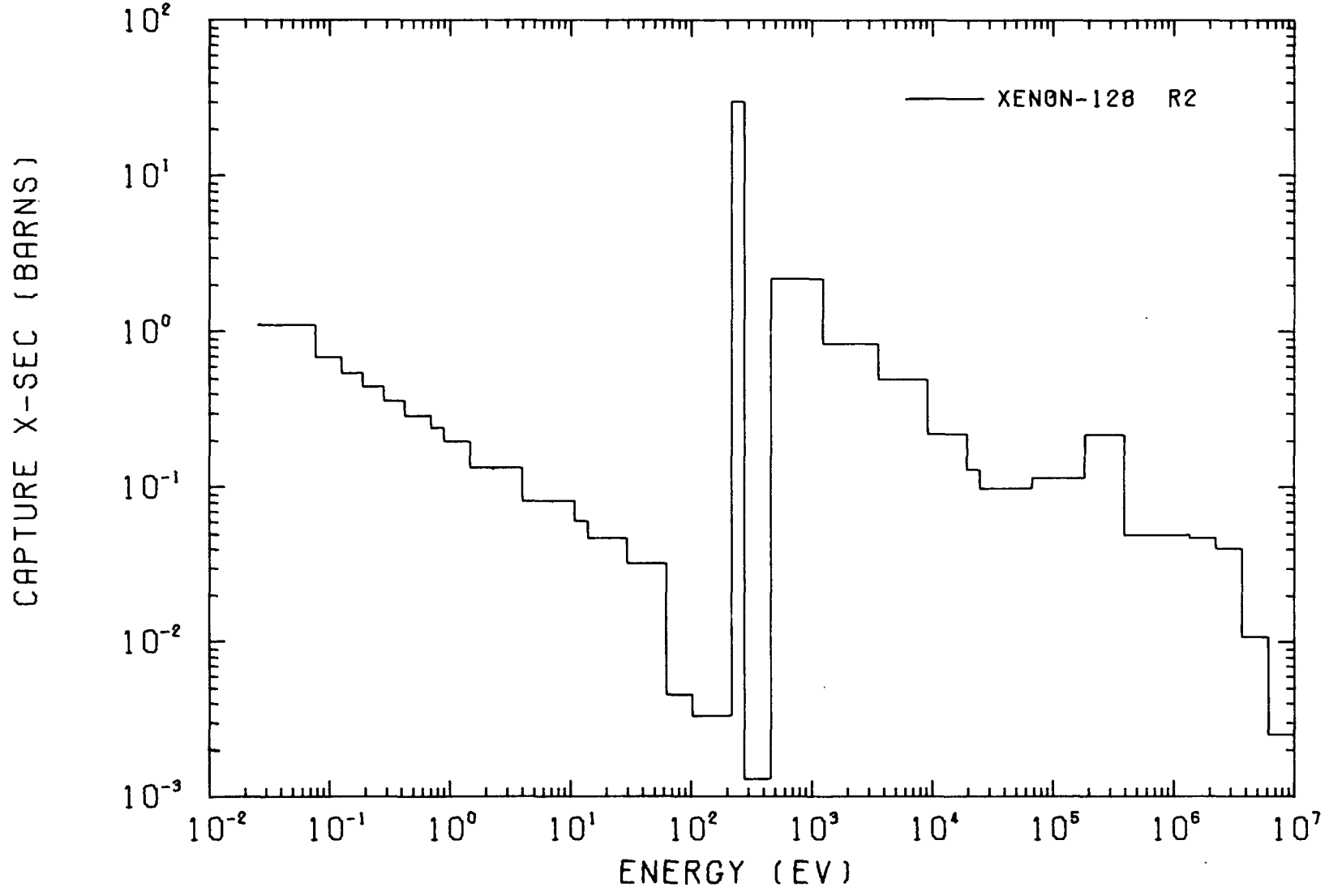

Figure 5. ^{128}Xe Spectrum Weighted Group Capture Cross Sections for the Volume-Averaged Plenum

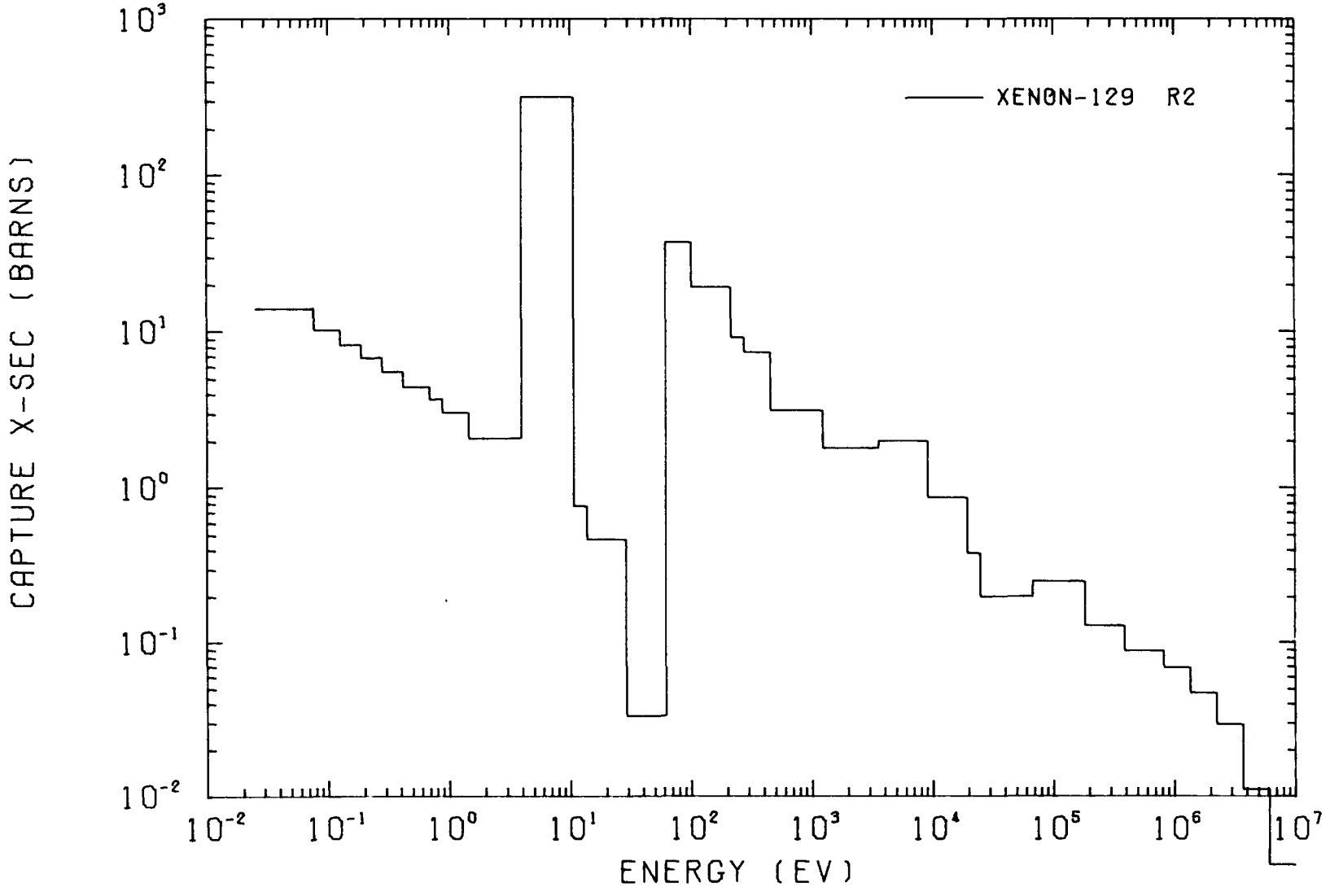

Figure 6. ^{129}Xe Spectrum Weighted Group Capture Cross Sections for the Volume-Averaged Plenum

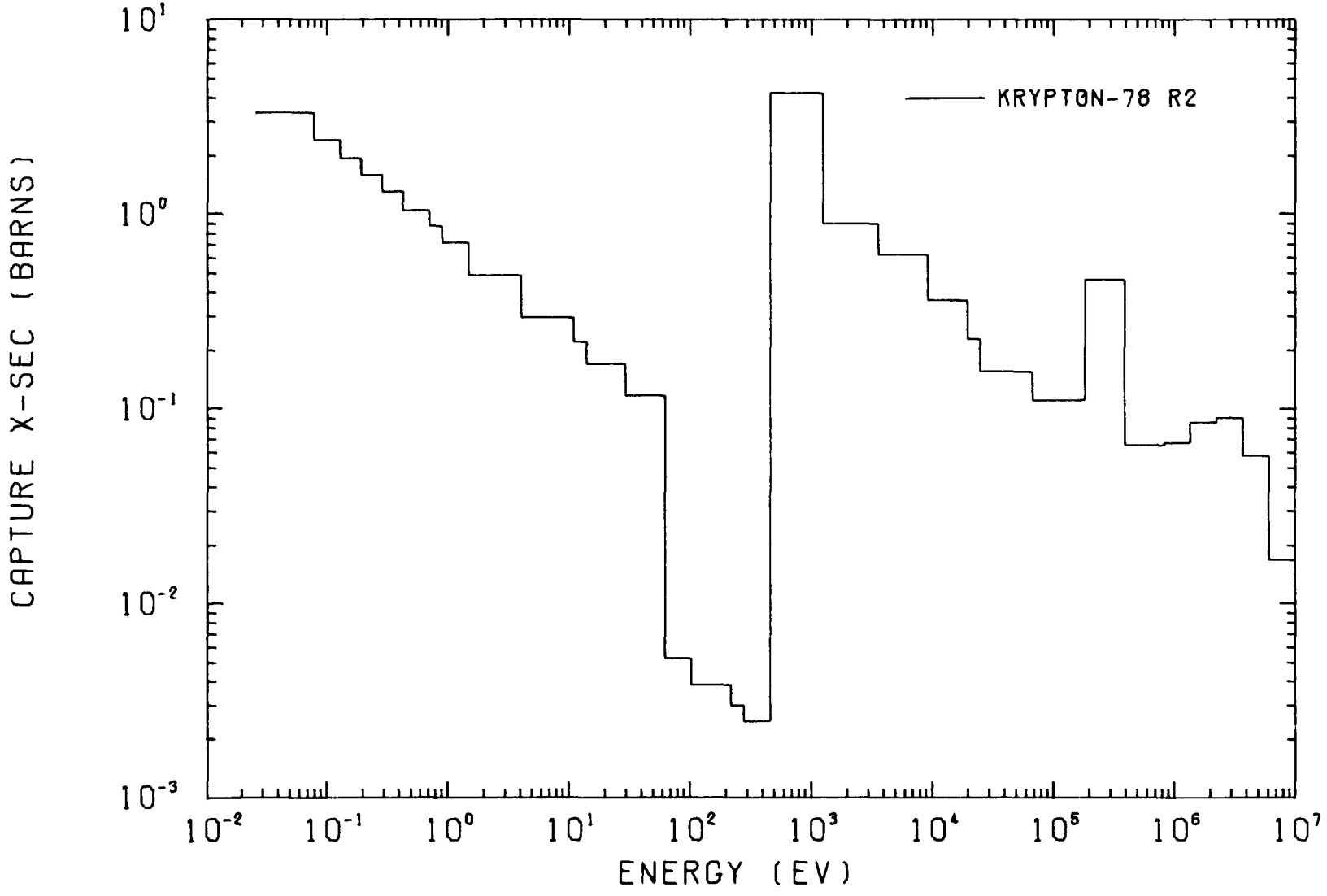

Figure 7. ^{78}Kr Spectrum Weighted Group Capture Cross Sections for the Volume-Averaged Plenum

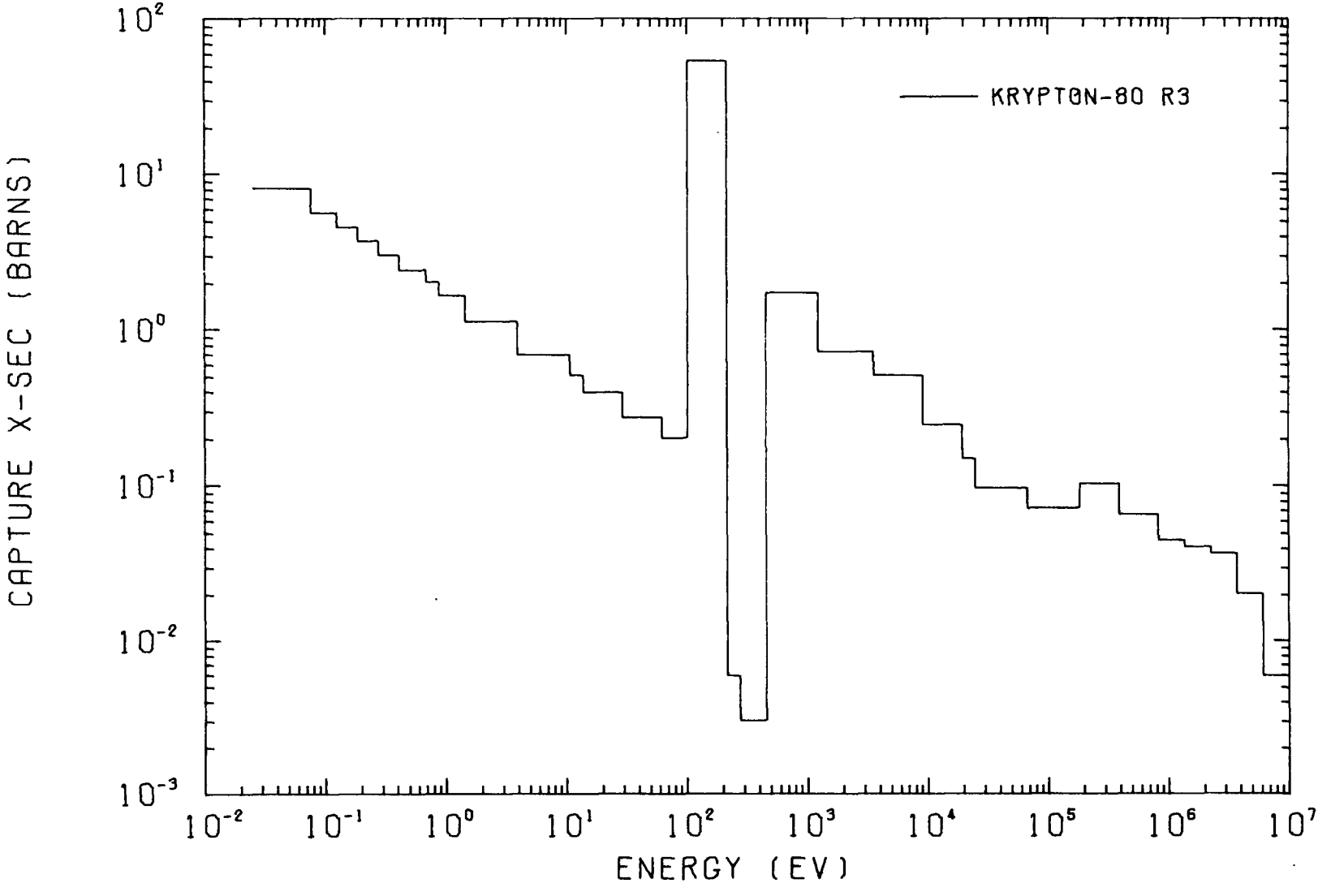

Figure 8. ^{80}Kr Spectrum Weighted Group Capture Cross Sections for the Volume-Averaged Plenum

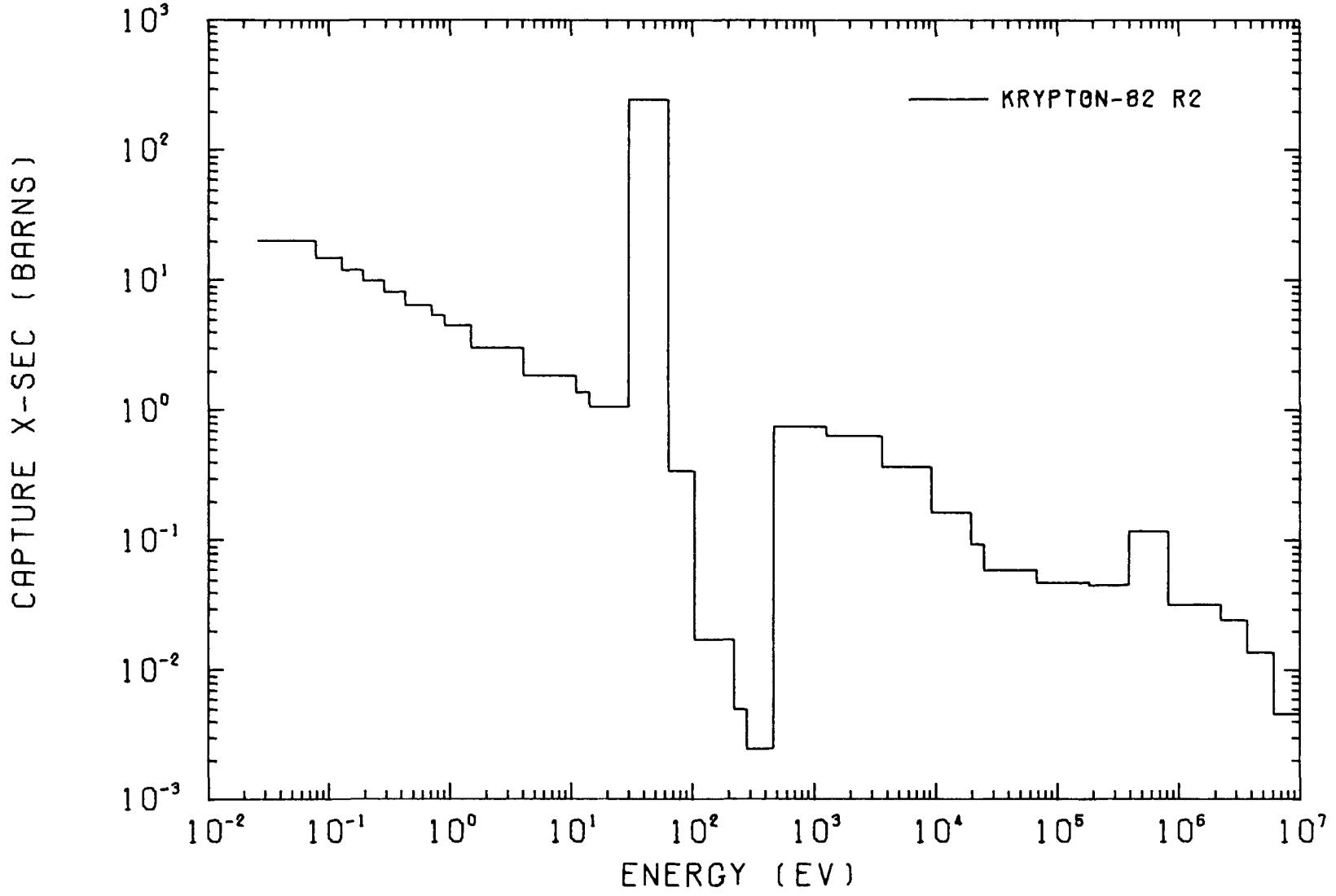

Figure 9. ^{82}Kr Spectrum Weighted Group Capture Cross Sections for the Volume-Averaged Plenum

TABLE 4

Spectrum Averaged Capture Cross Sections and Uncertainties For Positions In The FTR Gas Plenum

ISOTOPE	CROSS SECTION (BARNS)			
	Upper Plenum	Mid Plenum	Lower Plenum	Volume Averaged Plenum
Xe-124	178. ± 13.	127. ± 10.	52. ± 4.	93. ± 7.
Xe-126	3.4 ± .4	3.0 ± .4	2.0 $^{+.5}_{-.4}$	2.6 $^{+.5}_{-.4}$
Xe-128	1.1 $^{+.3}_{-.2}$	1.0 $^{+.3}_{-.2}$	.8 $^{+.3}_{-.2}$	.9 $^{+.3}_{-.2}$
Xe-129	22.1 ± 5.8	17.0 ± 4.4	8.2 ± 1.9	13.0 ± 3.1
Kr-78	.7 $^{+.3}_{-.2}$	.7 $^{+.3}_{-.2}$	.6 $^{+.4}_{-.3}$	.6 $^{+.4}_{-.3}$
Kr-80	4.6 ± .5	4.0 ± .5	2.3 ± .3	3.3 ± .3
Kr-82	17. ± 3.	14. ± 3.	7. ± 1.	10. ± 2.

The microscopic neutron capture rates for each noble gas isotope being considered are depicted in Figures 10 through 16. Radial distributions at three elevations in the plenum region are presented; and "68% confidence limits," as propagated from flux and cross sections uncertainties, are also included. The radial distributions are relatively smooth across the plenum region. Withdrawn safety rods and partially withdrawn control rods were not included in these analyses. Such perturbations can only be treated realistically with three-dimensional modeling of the FTR. It is expected that the presence of control material (B_4C) in the plenum region will distort the capture rate distributions significantly. However, it is expected that the presence of control rods would most likely depress and harden the neutron flux spectrum. Both these effects tend to reduce the tag-gas ratio changes so that the neglect of control rods provides conservative tag spacings.

The volume-averaged neutron capture rates for each isotope are listed in Table 5. Also included are the "68% confidence limits." The volume-averaged capture rate $\overline{\phi\sigma}$ is defined as

$$\overline{\phi\sigma} = \frac{\int_V \sum_{I=1}^{31} \phi_I \sigma_I \, dV}{\int_V dV} .$$

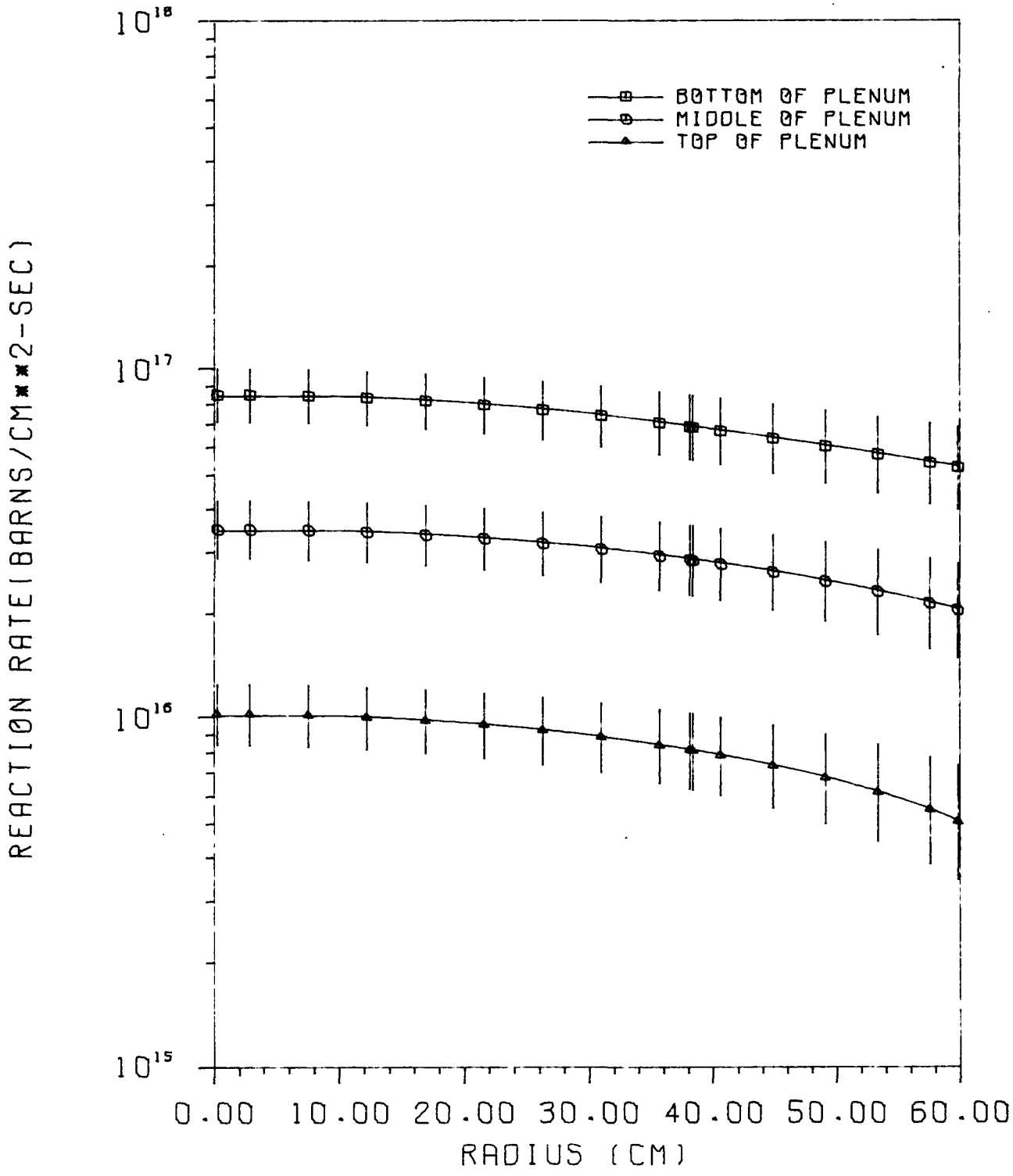

Figure 10. ^{124}Xe Reaction Rate Distribution in the Fission Gas Plenum

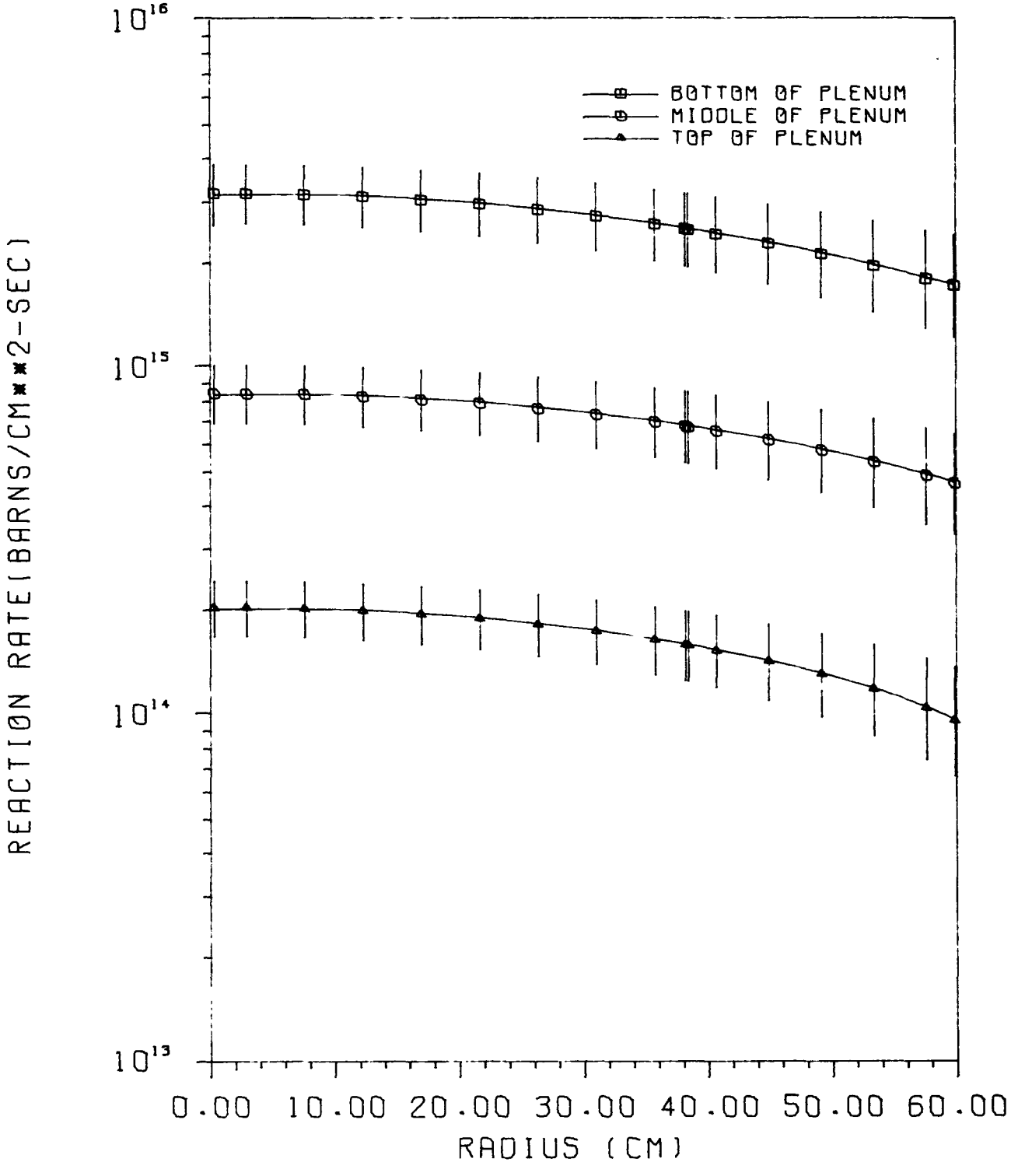

Figure 11. ^{126}Xe Reaction Rate Distribution in the Fission Gas Plenum

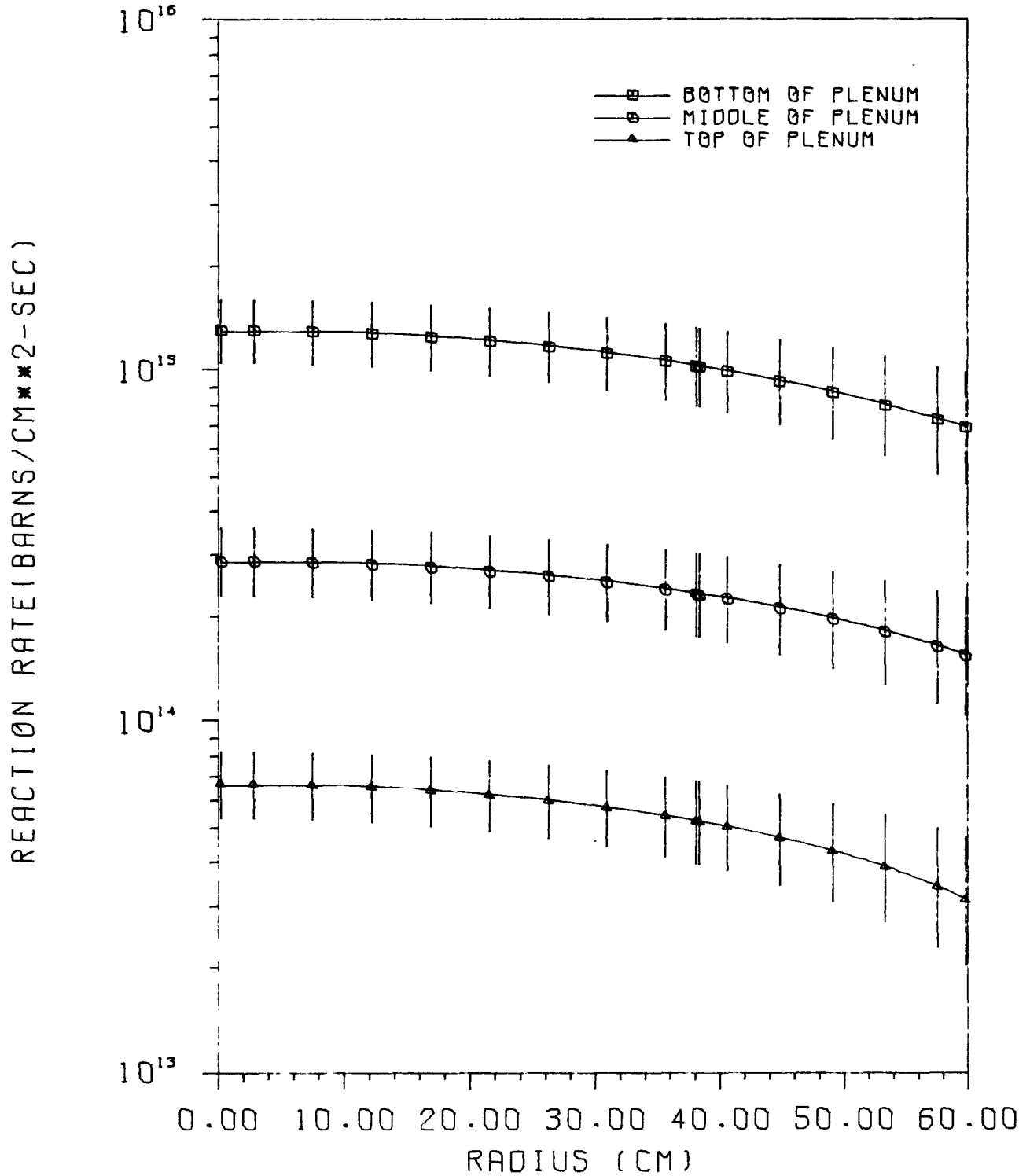

Figure 12. ^{128}Xe Reaction Rate Distribution in the Fission Gas Plenum

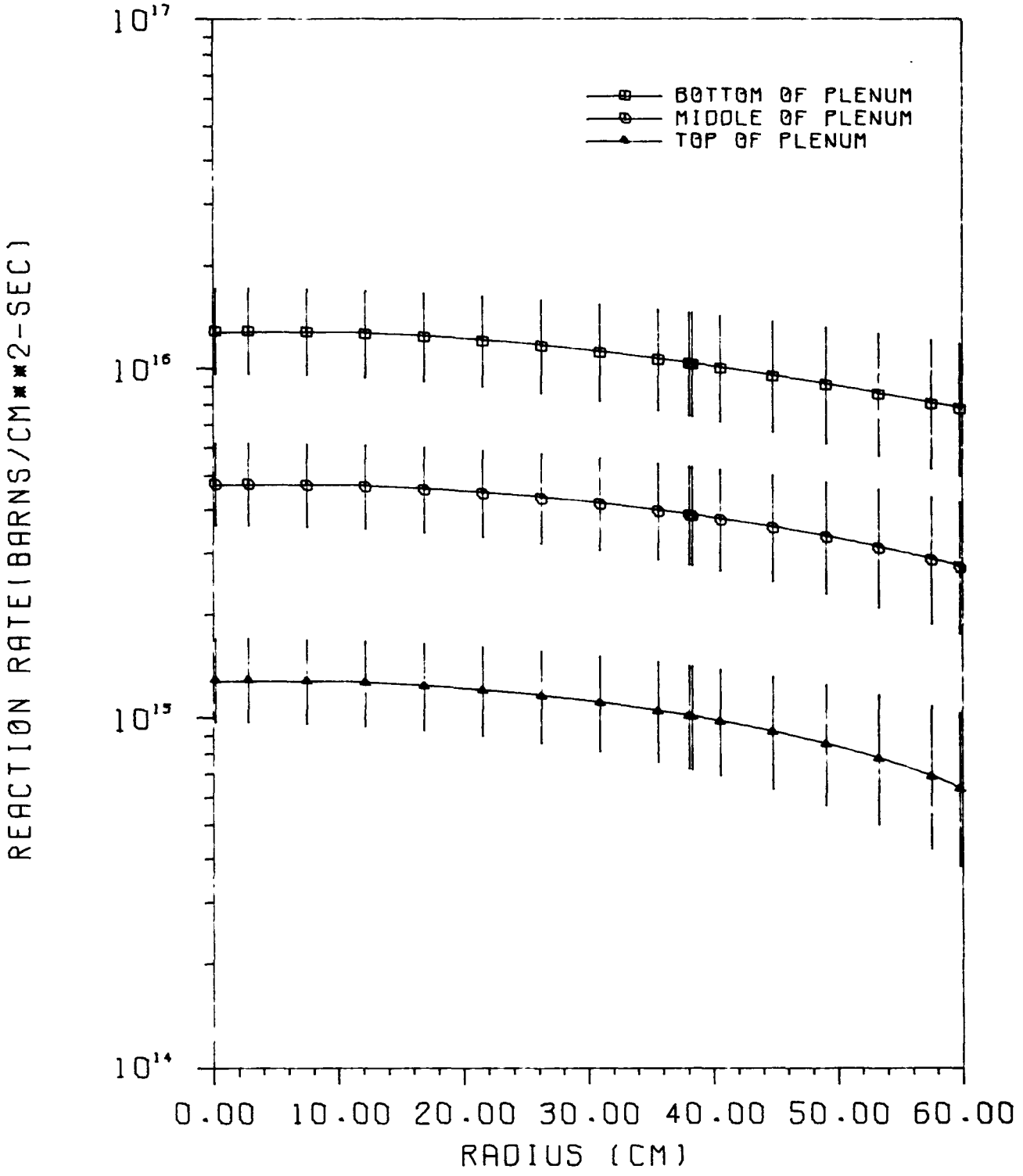

Figure 13. ^{129}**Xe Reaction Rate Distribution in the Fission Gas Plenum**

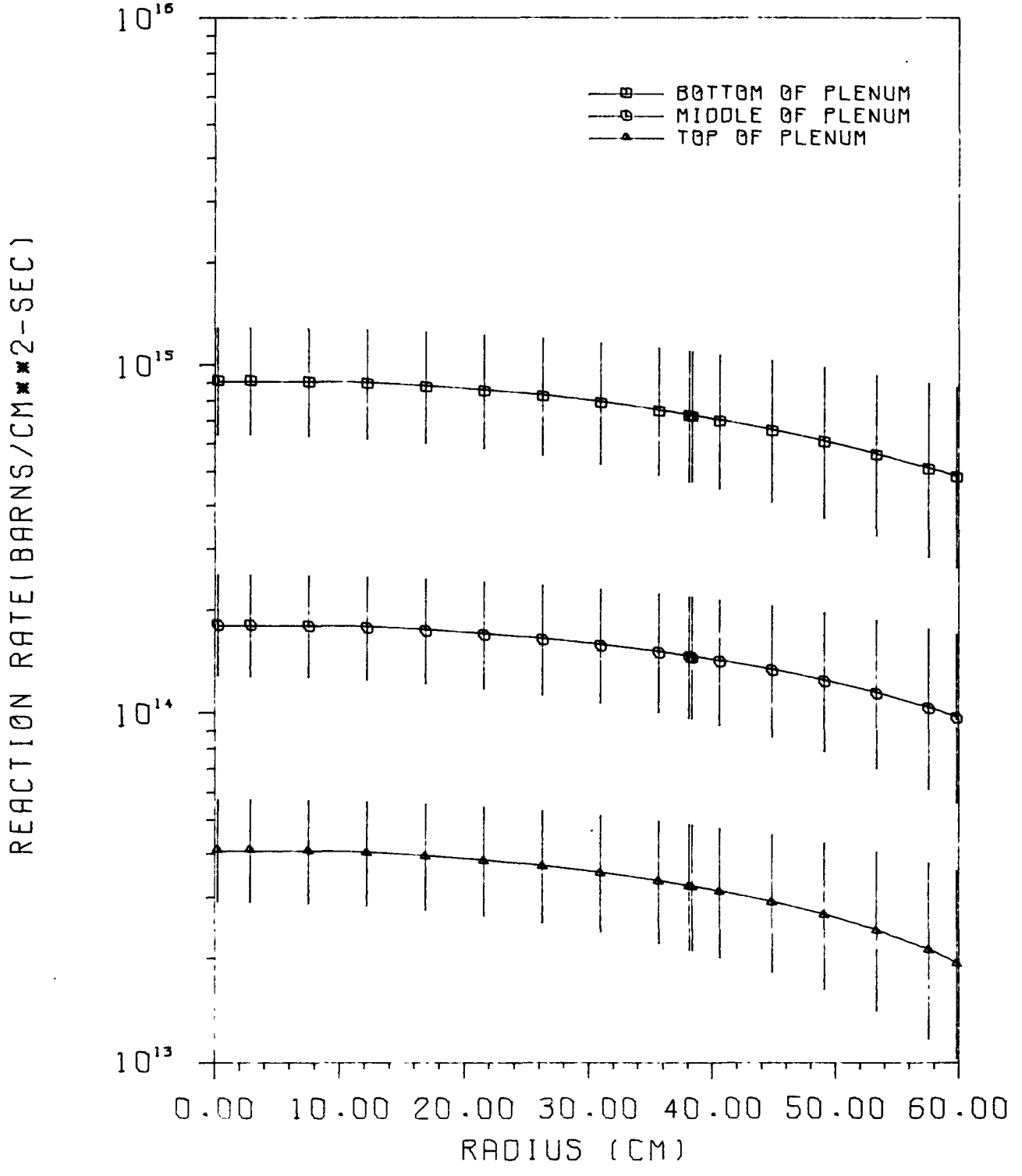

Figure 14. ^{78}Kr Reaction Rate Distribution in the Fission Gas Plenum

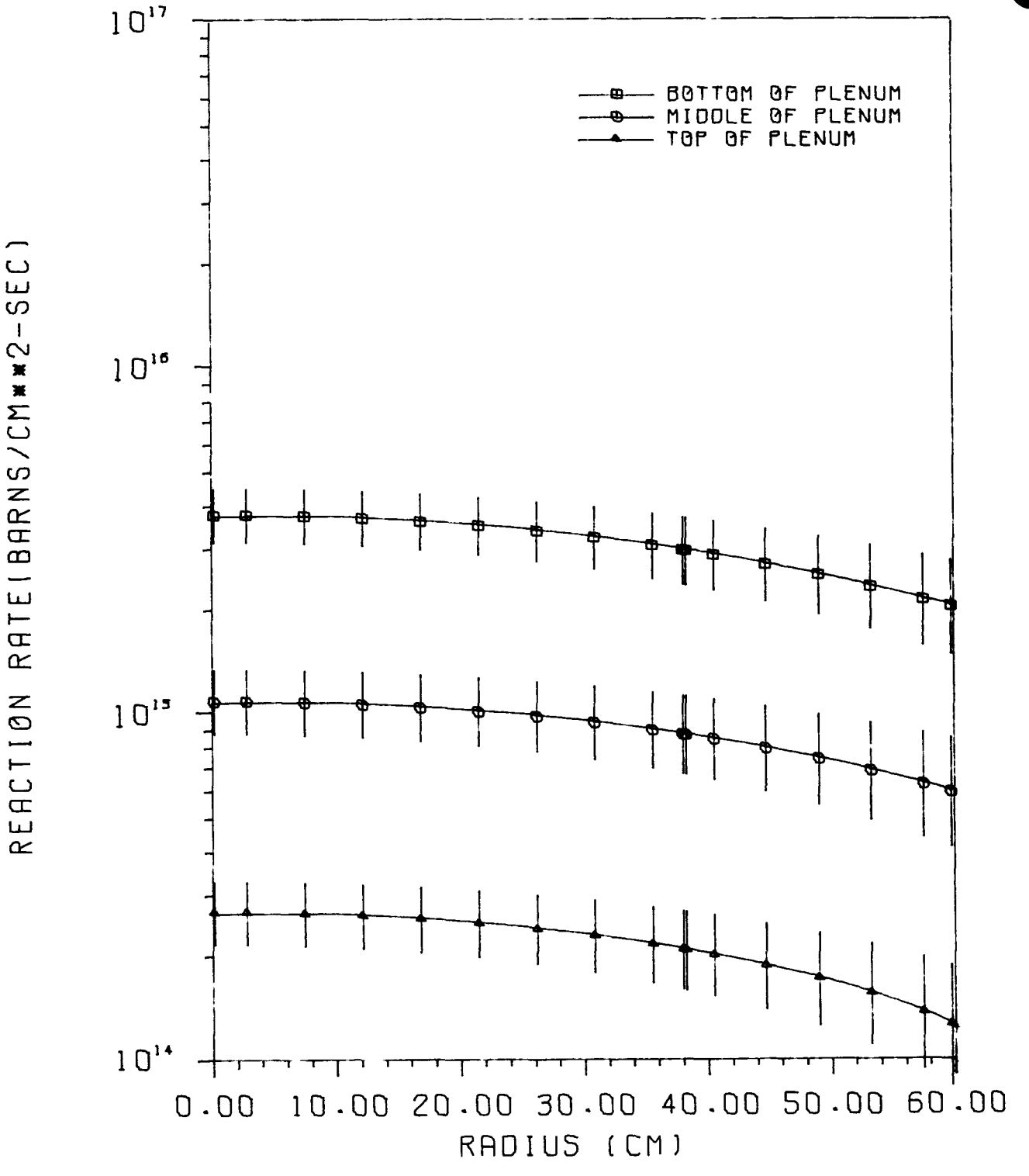

Figure 15. ^{80}Kr Reaction Rate Distribution in the Fission Gas Plenum

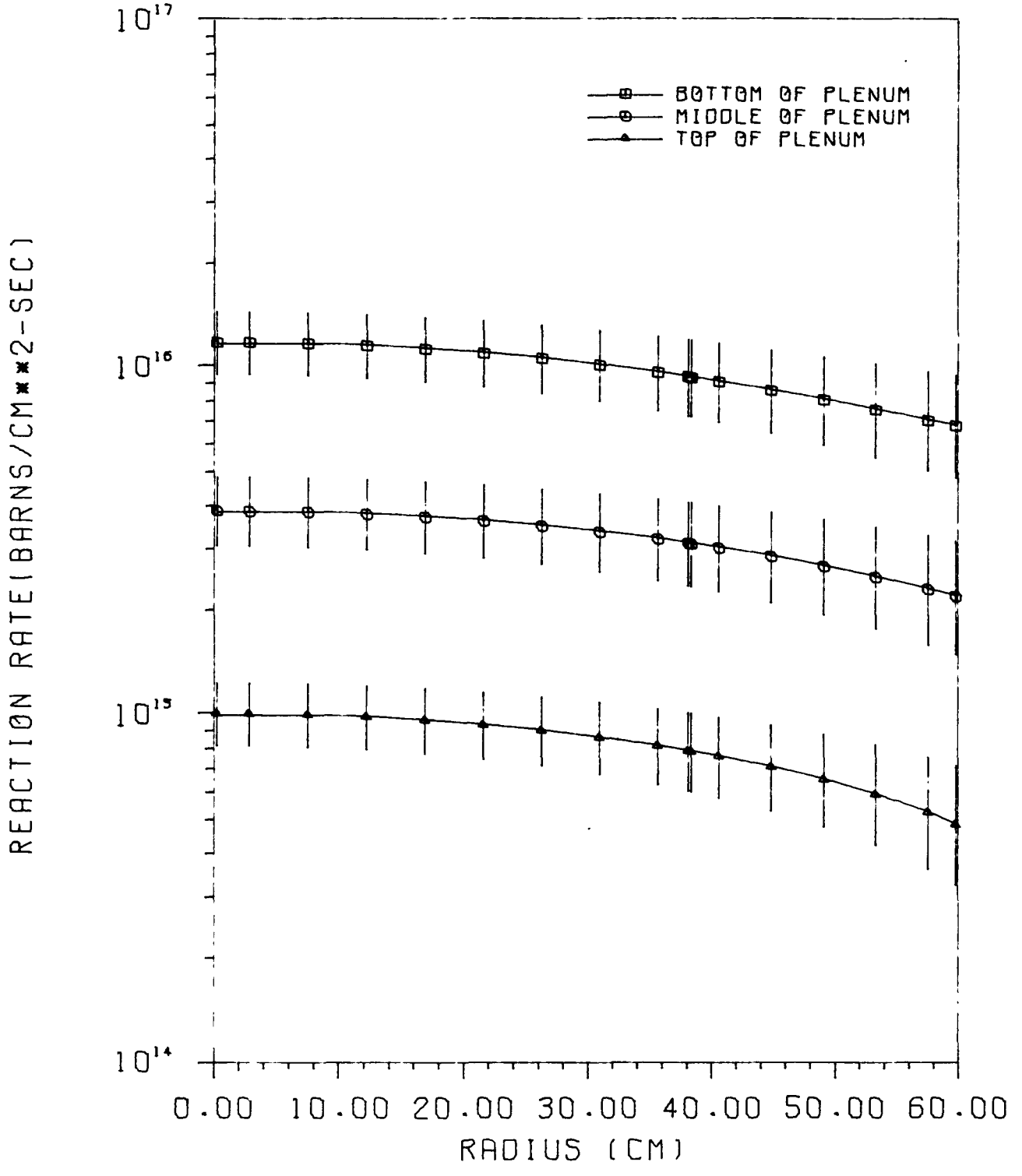

Figure 16. ^{82}Kr Reaction Rate Distribution in the Fission Gas Plenum

TABLE 5

Plenum Volume-Averaged Neutron Capture Rate of Gas Tag Isotopes

Isotope	$\overline{\phi\sigma}$ (barns/cm^2-sec)
^{78}Kr	$(2.29 \,^{+\,1.09}_{-\,0.74}) \times 10^{14}$
^{80}Kr	$(1.19 \,^{+\,0.31}_{-\,0.25}) \times 10^{15}$
^{82}Kr	$(4.05 \,^{+\,1.02}_{-\,0.81}) \times 10^{15}$
^{124}Xe	$(3.43 \,^{+\,0.77}_{-\,0.63}) \times 10^{16}$
^{126}Xe	$(9.55 \,^{+\,2.04}_{-\,1.69}) \times 10^{14}$
^{128}Xe	$(3.45 \,^{+\,0.85}_{-\,0.68}) \times 10^{14}$
^{129}Xe	$(4.88 \,^{+\,1.47}_{-\,1.13}) \times 10^{15}$

Equations defining the burnup rate of the gas tags and establishing the time variation of the isotopic ratios are described below. Uncertainties in the flux and cross sections are propagated to obtain uncertainties in the time variation of the gas tag ratios.

The time rate of change in the number of atoms of isotope Y due to neutron capture by atoms of isotope Y is defined by the following differential equation:

$$\frac{dN_Y}{dt} = -(\phi\sigma)_Y N_Y \quad , \qquad \text{(D-1)}$$

where $(\phi\sigma)_Y$ is the microscopic neutron capture rate for isotope Y and N_Y is the number of atoms of isotope Y at any time t. The solution of this equation for $N_y(t)$ is

$$N_Y(t) = N_Y^\circ \, e^{-(\phi\sigma)_Y t} \quad , \qquad \text{(D-2)}$$

where N_Y° is the number of Y atoms at time t=0. If we define $R_{X,Y}$ as the ratio of the number of X atoms to the number of Y atoms, it is clear that $R_{X,Y}$ as a function of exposure time t is

$$R_{X,Y}(t) = R^\circ_{X,Y} \, e^{[(\phi\sigma)_Y - (\phi\sigma)_X]t} \quad , \qquad \text{(D-3)}$$

where $(\phi\sigma)_X$ is the microscopic capture rate for isotope X and $R^\circ_{X,Y}$ is the ratio of the number of X atoms to the number of Y atoms at time t=0. If ϵ_X and ϵ_Y are defined as the uncertainties associated with $(\phi\sigma)_X$ and $(\phi\sigma)_Y$, respectively, then it can be shown that the uncertainty associated with $R_{X,Y}$ will take the following form:

$$\pm\epsilon^{(\pm)}_{R_{X,Y}}(t) = R^\circ_{X,Y} \, e^{[(\phi\sigma)_Y - (\phi\sigma)_X \pm (\epsilon_X^2 + \epsilon_Y^2)^{1/2}]t} - R_{X,Y}(t). \qquad \text{(D-4)}$$

Thus,

$$\left(R_{X,Y} \pm \epsilon^{(\pm)}_{R_{X,Y}}\right) = R^\circ_{X,Y} \, e^{[(\phi\sigma)_Y - (\phi\sigma)_X \pm (\epsilon_X^2 + \epsilon_Y^2)^{1/2}]\, t} \qquad \text{(D-5)}$$

defines the "68% confidence limits" for the time variation of the ratio $R_{X,Y}$.

The isotopic ratios of immediate interest are:

1. $^{129}Xe/^{124}Xe$
2. $^{128}Xe/^{124}Xe$
3. $^{128}Xe/^{126}Xe$
4. $^{129}Xe/^{128}Xe$
5. $^{80}Kr/^{78}Kr$
6. $^{82}Kr/^{78}Kr$
   $^{82}Kr/^{80}Kr$

Equations (D-3) and (D-5) are appropriate for six of the tags defined above. However, these equations do not hold for the ratio $^{129}Xe/^{128}Xe$. As ^{128}Xe burns up by neutron capture, atoms of ^{129}Xe are produced. Thus, the differential equation for the time rate of change in the number of ^{129}Xe atoms is

$$\frac{dN_9}{dt} = - (\phi\sigma)_9 N_9 + (\phi\sigma)_8 N_8 \qquad \text{(D-6)}$$

where N_9 and N_8 are, respectively, the number of ^{129}Xe and ^{128}Xe atoms at any time t; and, $(\phi\sigma)_9$ and $(\phi\sigma)_8$ are the microscopic neutron capture rate for ^{129}Xe and ^{128}Xe, respectively. The equation defining the time rate of change in N_8 is simply

$$\frac{dN_8}{dt} = - (\phi\sigma)_8 N_8 \quad , \qquad \text{(D-7)}$$

the solution of which is

$$N_8(t) = N_8^\circ \, e^{-(\phi\sigma)_8 t} \quad , \qquad \text{(D-8)}$$

where N_8° is the number of ^{128}Xe atoms at time t=0. Substitution of Equation (D-8) into Equation (D-6) yields the following solution for $N_9(t)$:

$$N_9(t) = N_9^\circ e^{-(\phi\sigma)_9 t} + \frac{N_8^\circ (\phi\sigma)_8}{(\phi\sigma)_9 - (\phi\sigma)_8} \left[e^{-(\phi\sigma)_8 t} - e^{-(\phi\sigma)_9 t} \right], \quad \text{(D-9)}$$

where N_9° is the initial concentration of ^{129}Xe. After some simplification, the ratio of N_9 to N_8 as a function of exposure time may be expressed as

$$R_{9,8} = R_{9,8}^\circ e^{[(\phi\sigma)_8 - (\phi\sigma)_9]t} + \frac{(\phi\sigma)_8}{(\phi\sigma)_9 - (\phi\sigma)_8} \left[1 - e^{[(\phi\sigma)_8 - (\phi\sigma)_9]t} \right]. \quad \text{(D-10)}$$

The exposure time range of interest in the FTR is from 0 to about 400 days (about 3×10^7 sec.). The difference $(\phi\sigma)_8 - (\phi\sigma)_9$ is about 10^{-9} $sec.^{-1}$ [see Table 5]. Thus, the exponents in Equation (D-10) are less than 10^{-2} for all exposure times of interest. Equation (D-10) can then be simplified to

$$R_{9,8} \simeq R_{9,8}^\circ \left\{ 1 + \left[(\phi\sigma)_8 - (\phi\sigma)_9 \right] t \right\} + (\phi\sigma)_8 t \quad . \quad \text{(D-11)}$$

(The approximation represented by Equation (D-10) is accurate to within 1% or less for all exposure times of interest.) From Equation (D-11), one can readily obtain $\varepsilon_{R_{9,8}}$ as a function of exposure time t; and the "68% confidence limits" for $R_{9,8}$ are:

$$\left(R_{9,8} \pm \varepsilon_{R_{9,8}}\right) = R_{9,8} \pm \left\{\left[R^{\circ}_{9,8}\ \varepsilon_9 t\right]^2 + \left[(1 + R^{\circ}_{9,8})\ \varepsilon_8\ t\right]^2\right\}^{1/2} , \qquad \text{(D-12)}$$

where ε_9 and ε_8 are the uncertainties associated with $(\phi\sigma)_9$ and $(\phi\sigma)_8$, respectively.

Further simplifications of $R_{9,8}$ may be made by examining Equation (D-11). Note that the first term on the right is simply the expansion, to first order terms, of Equation (D-3). The second term on the right, $(\phi\sigma)_8 t$, accounts for the buildup of ^{129}Xe by capture in ^{128}Xe. Substitution of the values for the capture rates in Equation (D-11) yields

$$R_{9,8} \simeq R^{\circ}_{9,8}\ (1 - 4.5 \times 10^{-9} t) + 3.4 \times 10^{-10} t. \qquad \text{(D-13)}$$

For any initial value $R^{\circ}_{9,8}$, the contribution to $R_{9,8}$ of the buildup term is a maximum at the largest value of t; i.e., at t=400 days (3.5×10^7 sec.). Thus,

$$R_{9,8}\ (400\ \text{days}) \simeq 0.84\ R^{\circ}_{9,8} + 0.012 \qquad \text{(D-14)}$$

and it is obvious that the buildup term must be taken into account if $R^{\circ}_{9.8}$ is less than about 0.1. For values of $R^{\circ}_{9,8}$ greater than 0.1 the contribution from the buildup term is insignificant for all values of exposure time.

Equations (D-3), (D-5), D-11) and (D-12) have been solved as a function of exposure time at 400 MW for the volume-averaged neutron capture rates reported in Table 5. The results are plotted in Figures 17-24 where the dashed lines represent the "68% confidence limits." The solutions have been normal-

ized to an initial isotopic ratio of one. However, the distribution may be scaled uniformily according to the magnitude of the initial ratio. If the initial ratio of the $^{129}Xe/^{128}Xe$ tag is less than 0.1, then adjustments to the scaled results must be made by adding the results in Figure 24 to the results scaled from Figure 20. The results depicted in Figure 24 are not dependent upon $R^{\circ}_{9,8}$; therefore, they may be added directly.

E. FUTURE ANALYSES

Further neutronic analyses are required to establish the effect of material perturbations in the fission gas plenum region. Withdrawn safety rods and control rods will grossly distort the isotopic reaction rate distribution presented in Section D. This implies that the time distribution of gas tag isotopic ratios will be spatially dependent and that initial tag composition should be selected and positioned in the FTR core to account for these perturbations. A three-dimensional analysis of the microscopic capture rate for each isotope should be made. This calculation should include all material perturbation of importance, and it should yield microscopic capture rate averaged over each FTR fuel assembly plenum.

Finally, the production of ^{128}Xe and ^{82}Kr via fission in FTR fuel must be included into the analyses. Although ^{128}Xe is not formed directly by fission, the capture of neutrons by the ^{127}I fission product may yield a significant ^{128}Xe production. Similar arguments apply to the ^{82}Kr isotope, which is formed by neutron capture in ^{81}Br, a direct fission product.

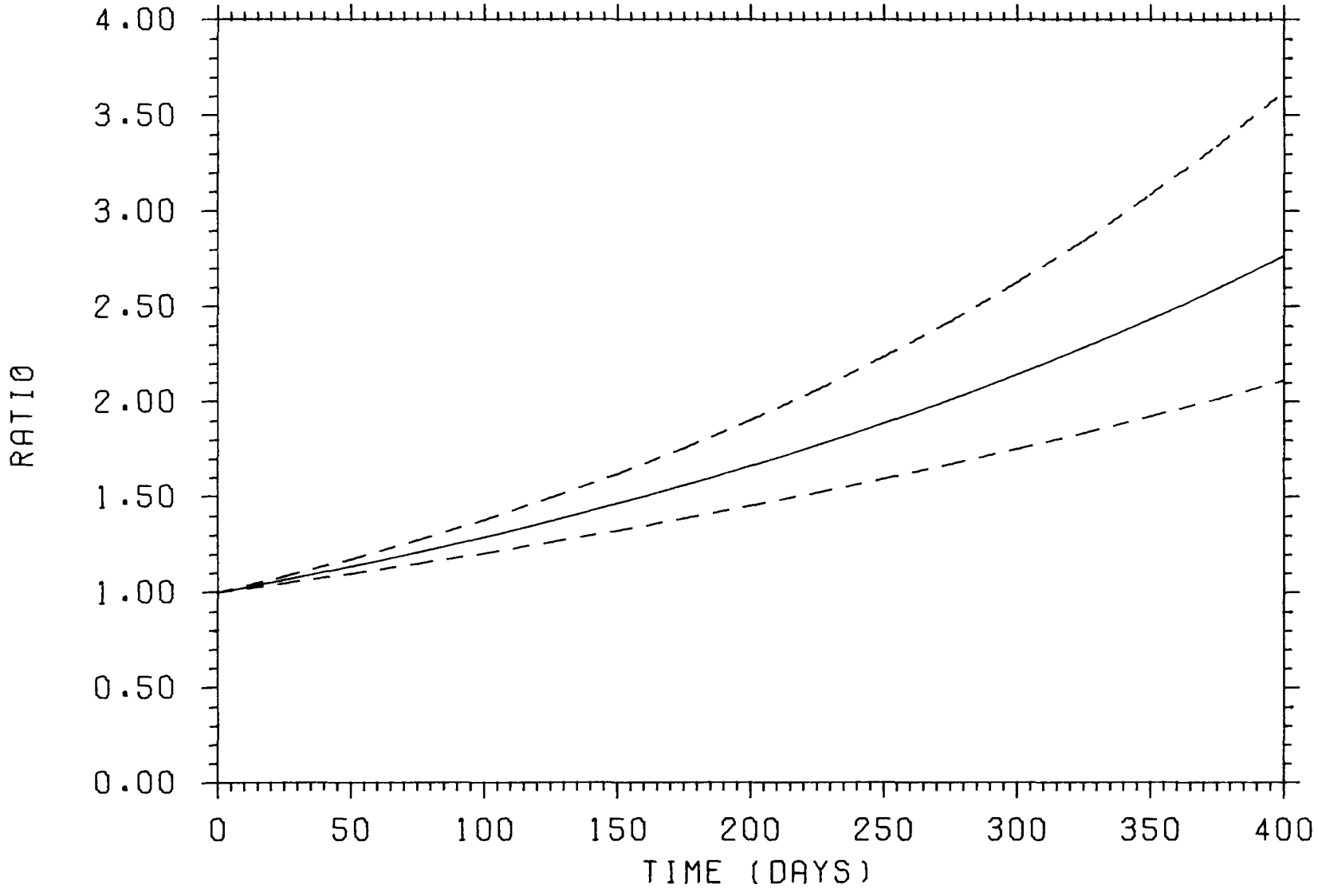

Figure 17. Ratio of $^{129}Xe/^{124}Xe$ vs Exposure Time at 400 MW

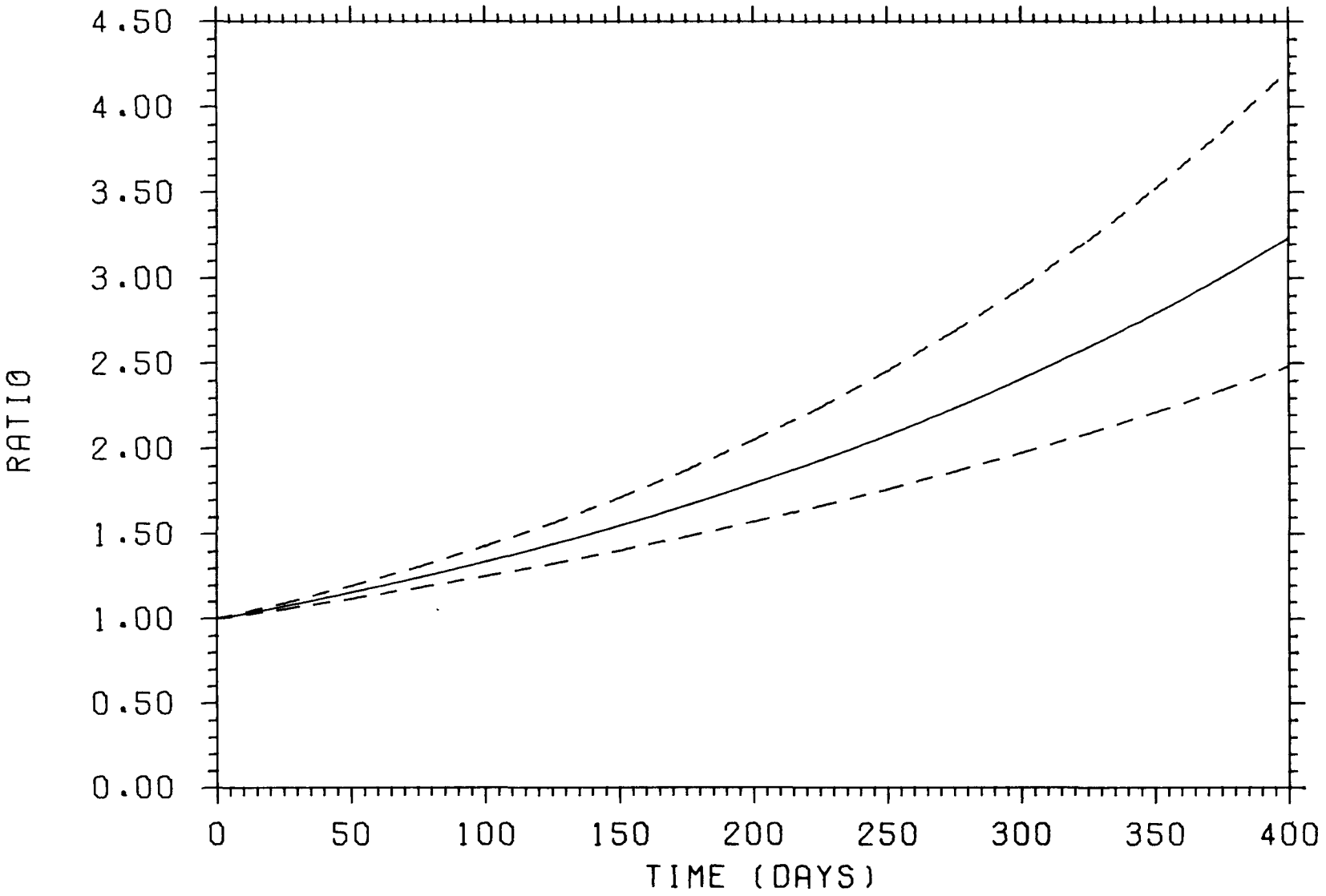

Figure 18. Ratio of $^{128}Xe/^{124}Xe$ vs Exposure Time at 400 MW

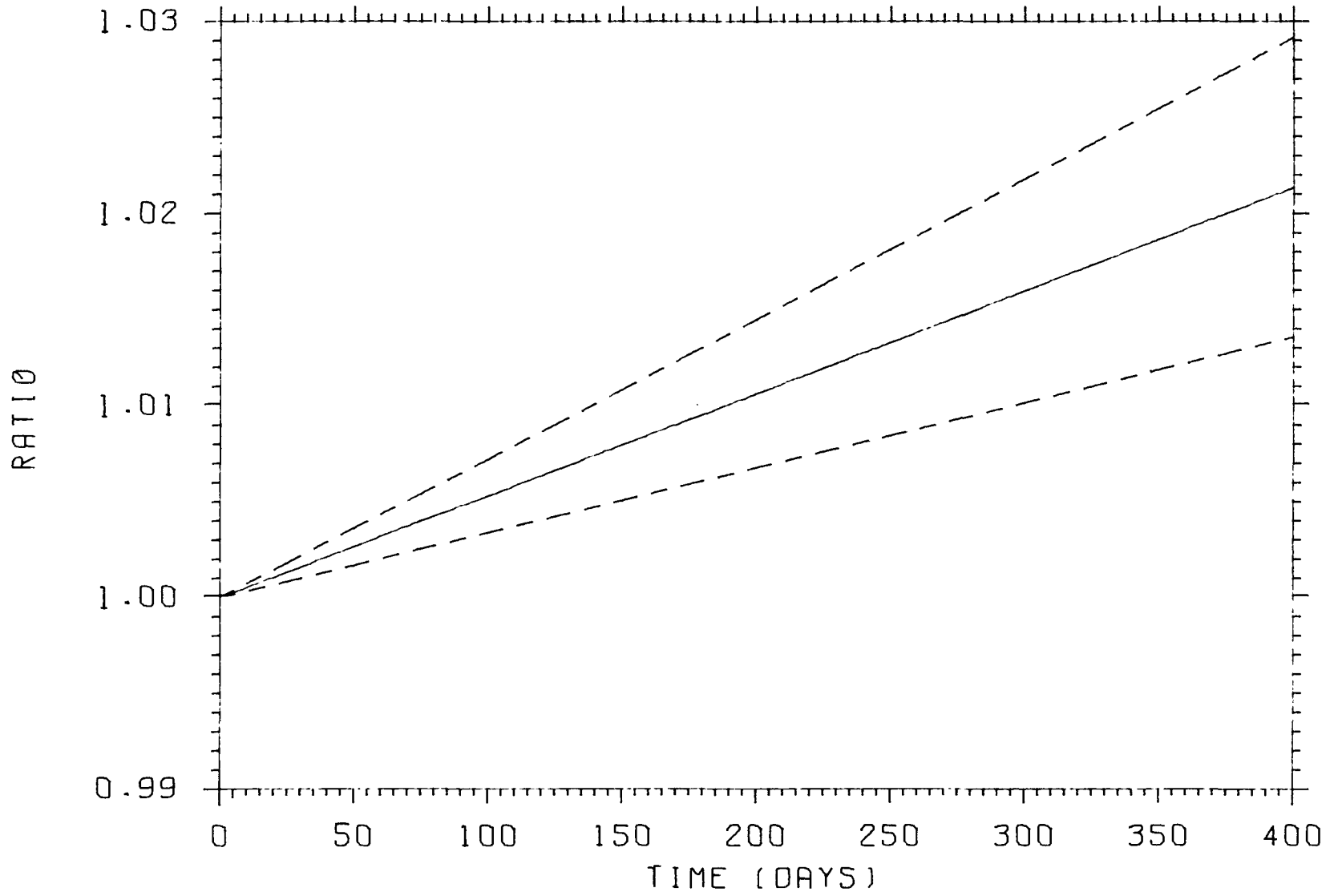

Figure 19. Ratio of $^{128}Xe/^{126}Xe$ vs Exposure Time at 400 MW

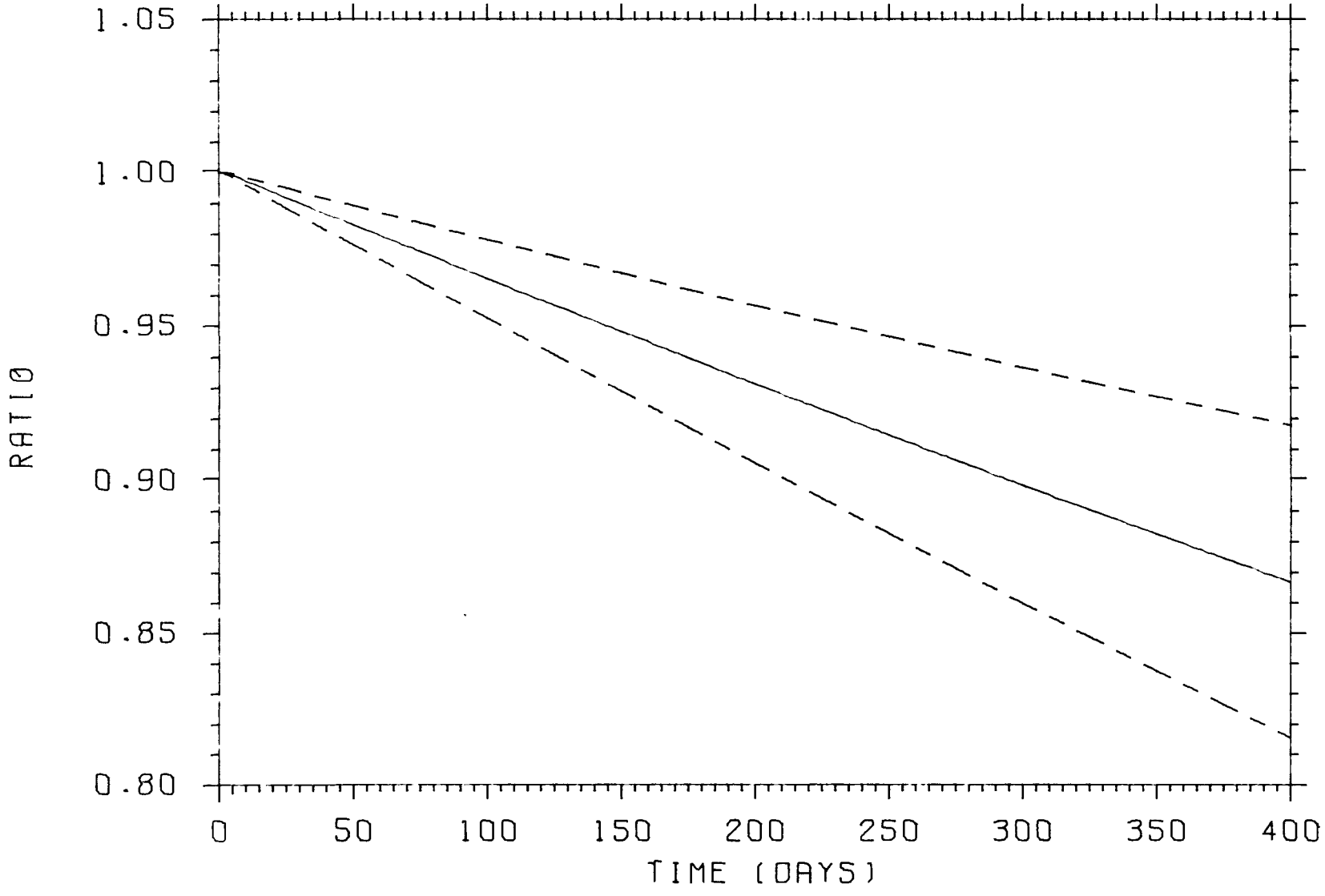

Figure 20. Ratio of $^{129}Xe/^{128}Xe$ vs Exposure Time at 400 MW

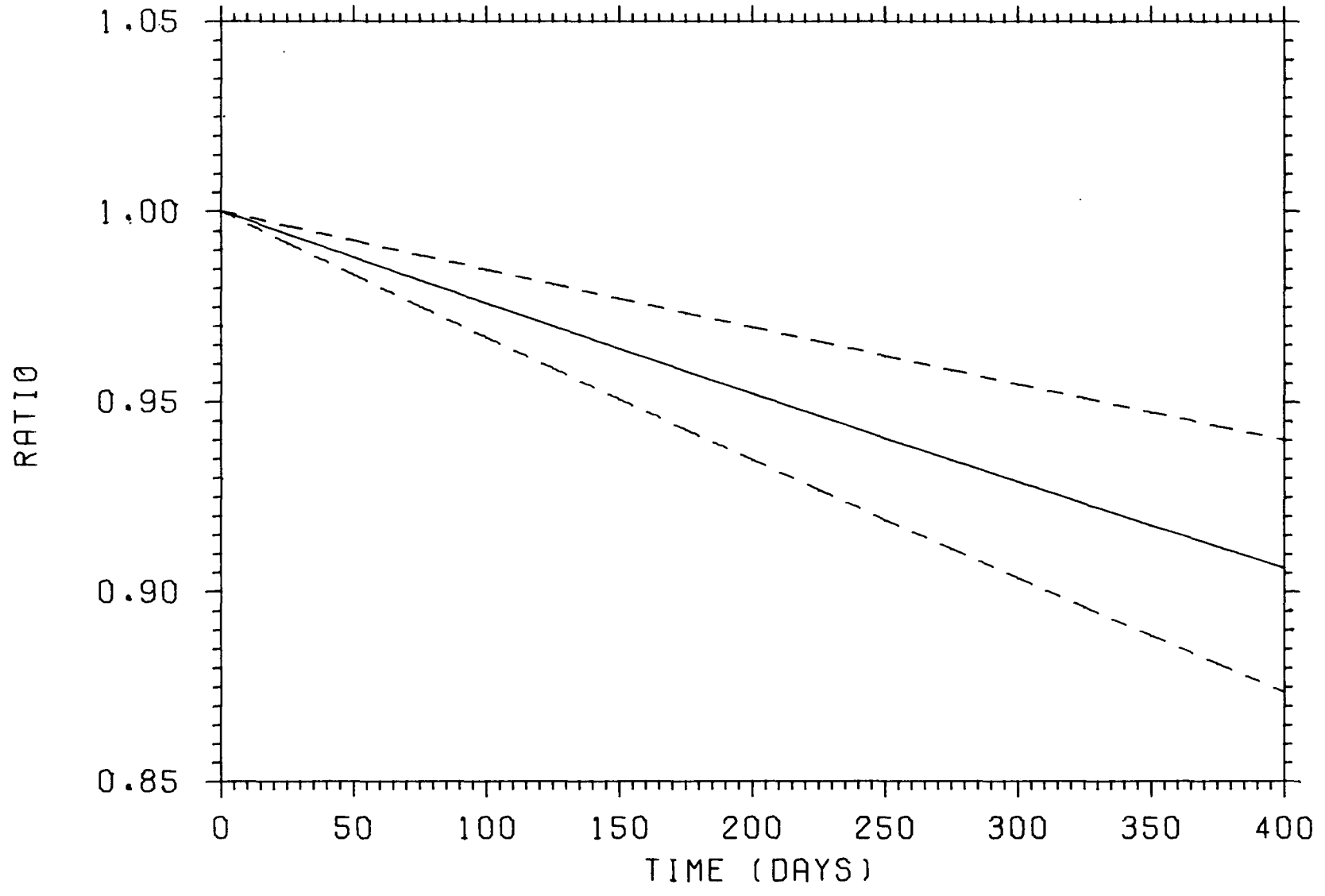

Figure 21. Ratio of $^{82}Kr/^{80}Kr$ vs Exposure Time at 400 MW

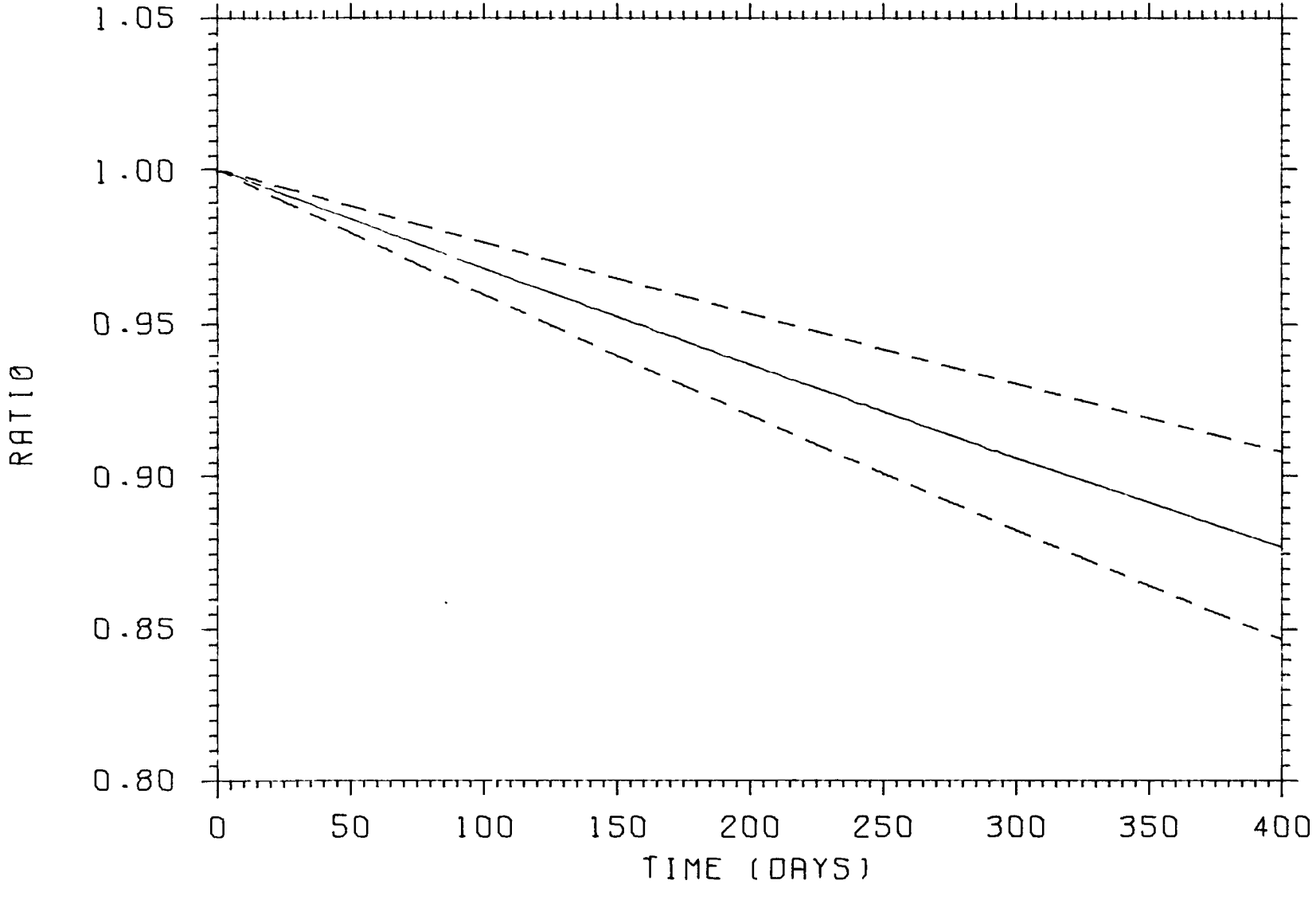

Figure 22. Ratio of $^{82}Kr/^{78}Kr$ vs Exposure Time at 400 MW

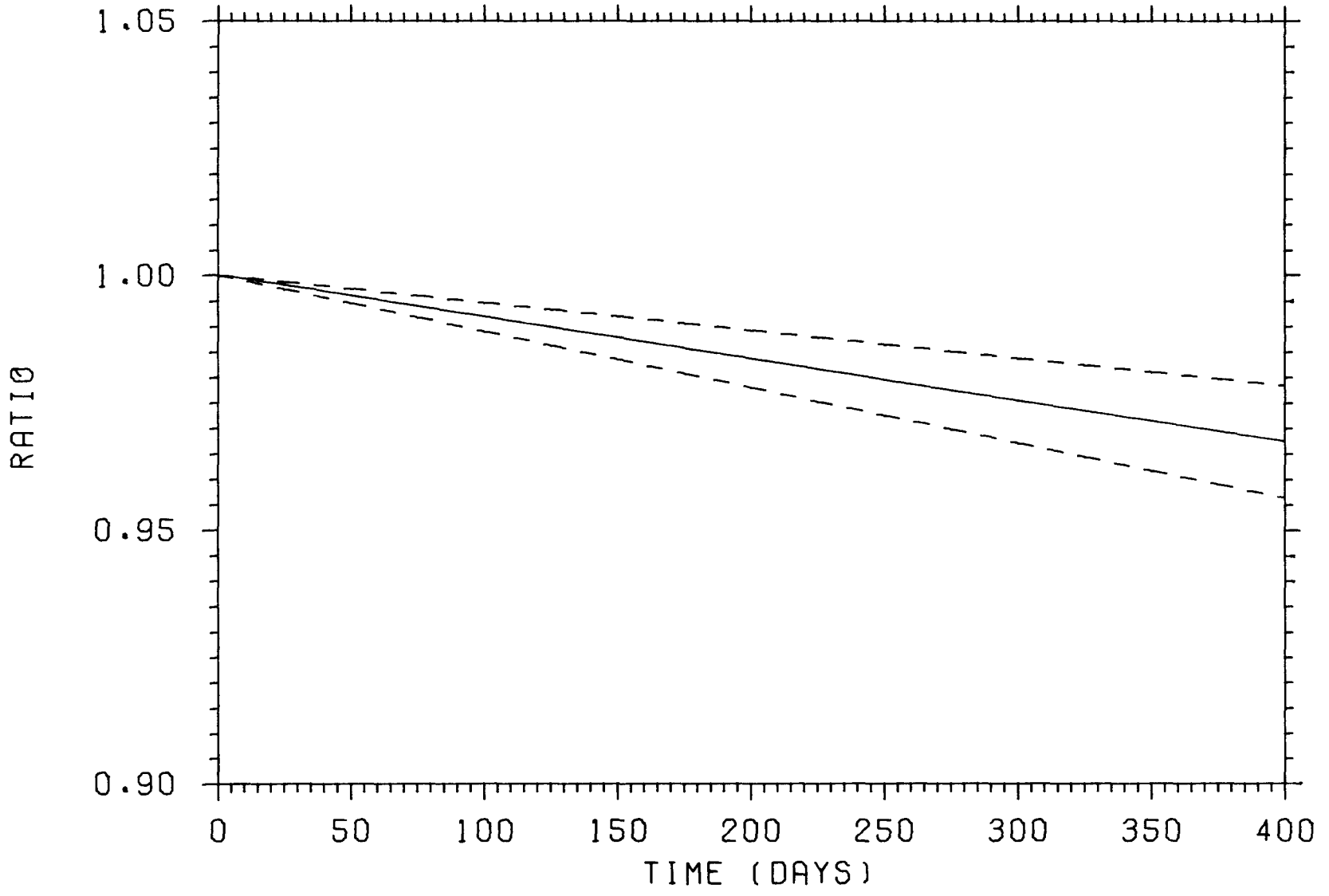

Figure 23. Ratio of $^{80}Kr/^{78}Kr$ vs Exposure Time at 400 MW

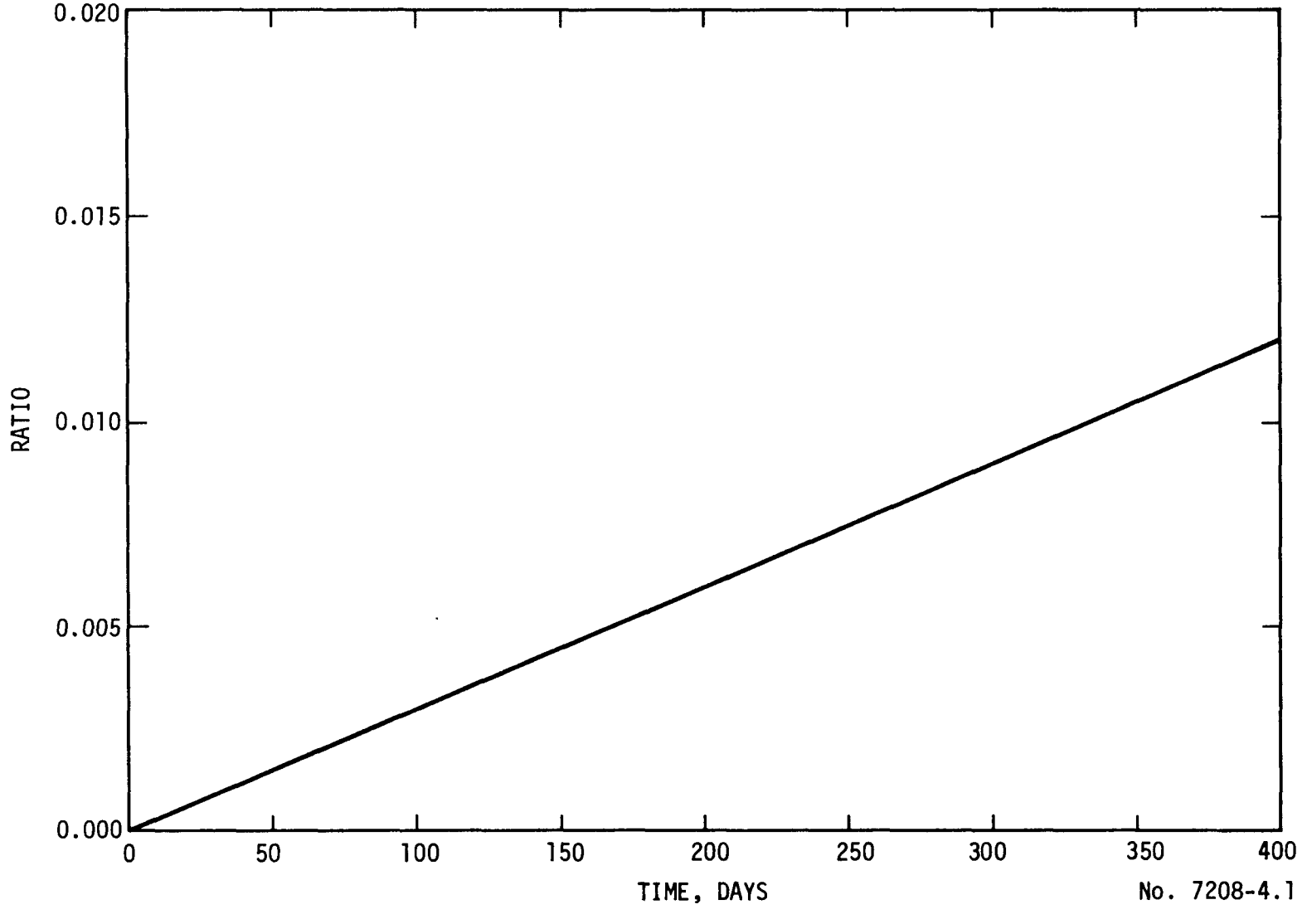

Figure 24. Ratio of $^{129}Xe/^{128}Xe$ due to Buildup of ^{129}Xe by Neutron Capture in ^{128}Xe.

References

1. P. B. Henault, W. J. Larson, R. E. Rice, and C. W. Wilkes, "Progress in Xenon Tagging," Trans. Am. Nucl. Soc., 13, 797 (1970).

2. D. R. Marr, "A User's Manual for 2DBS, A Diffusion Theory Shielding Code," BNWL-1291, Battelle-Northwest (1970).

3. E. T. Boulette, "Analysis of ZPPR/FTR Shield Experiments: Neutron Distribution," WHAN-FR-12, WADCO Corp. (October 1970).

4. E. T. Boulette, "Streaming Analysis for the FTR Fission Gas Plenum Region," HEDL-TME 72-52, Hanford Engineering Development Laboratory,

5. D. R. Marr, "A Discrete Ordinates Study of Neutron Attenuation in Sodium," Trans. Am. Nucl. Soc., 11, 700 (1968).

6. E. T. Boulette, "ZPPR/FTR-2 Shield Experiments: Neutron Distributions," Trans Am. Nucl. Soc., 13, 399 (1970).

7. F. A. Schmittroth, "Theoretical Calculations of Fast Neutron Capture Cross Sections," HEDL-TME-71-106, Hanford Engineering Development Laboratory, August 1971.

8. Yu. P. Popov and M. Florek, "(n,α) Reactions on Resonance Neutrons Close to Shells with N=50, and Z=50," International Atomic Energy Agency, INDC(CCP)-7/U, February 1970.

9. D. P. Mann, and W. W. Watson, "Total Neutron Cross Section of Xenon and Krypton," Phys. Rev., 116, 1516 (1959).

10. R. Ribon, B. Cauvin, H. Derrien, A. Michaudon, E. Silver and J. Trochon, "Etude de Quelques Sections Efficaces Neutroniques Total et de Diffusion dans le Domaine des Resonances," Nuclear Data for Reactors, Vol. 1, 1967.

11. M. Bresesti, F. Cappellani, A. M. Del Turco and E. Orvini, "The Thermal Neutron Capture Cross Section and the Resonance Capture Integral of Xe-124," Nucl. Chem., 26, 9 (1964).

12. J. G. Bradley and W. H. Johnson, "The Thermal-Neutron Capture Cross Section and Resonance Capture Integral of Krypton-80," Nucl. Sci. Eng., 47, 151 (1972).

13. M. Bresesti, F. Cappellani, A. M. Del Turco, H. Neumann and E. Orvini, "Neutron Capture Cross Sections of Xe-126 and Xe-136," Nucl. Chem., 27, 1175 (1965).

14. E. Kondaiah, N. Ranajumar and R. W. Fink, "Thermal Neutron Activation Cross Sections for Kr and Xe Isotopes," Nucl. Phys., A 120, 329 (1968).

15. F. Schmittroth, "Neutron Resonance Spacing For Spherical Nuclei," to be published.

16. F. Schmittroth, "Analysis of Errors in Computed Integral Cross Section Due to Fluctuating Resonance Paramaters," HEDL-TME-72-99, Hanford Engineering Development Laboratory, July 1972.

17. R. E. Schenter and F. Schmittroth, "Noble Gas Cross Section Calculations and Uncertainties For Fuel Failure Location Studies," to be published.

DISTRIBUTION

No. of Copies

OFFSITE

21 AEC Division of Reactor Development and Technology

Director, RDT
Asst Dir, Project Management
Asst Dir, Nuclear Safety
Asst Dir, Plant Engineering
Asst Dir, Reactor Engineering
Asst Dir, Reactor Technology
FFTF Project Manager
LMFBR Program Manager
EBR-II Program Manager
Chief, Liquid Metal Projects Br
Chief, Analysis and Evaluation Br
Chief, Fast Reactor Safety Br
Chief, Fuel Recycle Br
Chief, Reactor Physics Br
Chief, Instrumentation & Control Br
Chief, Liquid Metal Systems Br
Chief, Core Design Br
Chief, Fuel Engineering Br
Reactor Physics Br
PB Hemmig
RJ Neuhold
Core Design Br
TE Murley

2 AEC Division of Technical Information Extension

17 Manager, Technical Information Center (ACRS/TIC)

5 AEC Site Representatives

Argonne National Laboratory-ID
Argonne National Laboratory-AR
Atomics International
General Electric Company
Westinghouse Electric Corporation

No. of Copies

OFFSITE

1 Aerojet Nuclear Company

P.O. Box 1845
Idaho Falls, Idaho 83401
RM Brugger

2 Argonne National Laboratory

R Avery
OMFBR Program Office

1 Atomic Power Development Associates, Inc.

1911 First Street
Detroit, Michigan 48226
JB Nims

2 Atomics International

H Alter
HA Morewitz

2 Babcock & Wilcox Company

Old Forest Road
Lynchburg, Virginia 24505
DH Roy
AZ Livolzi

4 Brookhaven National Laboratory

M Drake
S Pearlstein
M Bhat
A Prince

1 Combustion Engineering, Inc.

P.O. Box 500
Windsor, Connecticut 06090
JJ Prabulos, Jr.

2 General Electric Company

Breeder Reactor Division Operation
P Greebler
B Wolfe

No. of Copies

OFFSITE

1 Gulf General Atomic Inc.

P.O. Box 608
San Diego, California 92112
R Dahlberg

2 Lawrence Livermore Laboratory

P.O. Box 808
Livermore, California 94550
RJ Howerton
D Gardner

1 Los Alamos Scientific Laboratory

GH Best

4 Oak Ridge National Laboratory

CE Clifford FR Mynatt
WO Harms AM Perry

1 Gulf United Nuclear Fuels Corporation

Grasslands Road
Elmsford, New York 10523
JR Tomonto

5 Westinghouse Electric Corporation

Advanced Reactors Division
MW Dyos T Pitterle
PF Fox YS Tang
RJ Slember

ONSITE HANFORD

1 RDT Site Office

PE Standerfer

2 Battelle Northwest Laboratory

LC Schmid
Technical Information Files

No. of
Copies

ONSITE HANFORD

3 AEC, Richland Operations Office

TM Nemzek
RM Poteat
JM Shivley

Westinghouse Hanford

82

QL Baird
RA Bennett
WE Black
AG Blasewitz
ET Boulette (10)
WL Bunch
JP Burn
RJ Cash
RR Derusseau
EA Evans
JA Figg
RM Fleischman
RW Hardie
RA Harris
RE Heineman
RJ Hennig
FJ Holt
DI Hulbert
RB Kidman
HT Knight
FJ Leitz
WW Little
DR Marr
WN McElroy
JV Nelson
BH Noordhoff
LD O'Dell
RP Omberg
RB Rothrock
RE Schenter (10)
F Schmittroth (10)
DW Shannon
A Squire
JW Upton
AE Waltar
SA Weber
WR Wykoff
Document Control (15)
Technical Publications (2)